Polarized E-cadherin endocytosis directs actomyosin remodeling during embryonic wound repair

Miranda V. Hunter,[1] Donghoon M. Lee,[1] Tony J.C. Harris,[1] and Rodrigo Fernandez-Gonzalez[1,2,3]

[1]Department of Cell and Systems Biology, University of Toronto, Toronto, Ontario M5S 3G5, Canada
[2]Institute of Biomaterials and Biomedical Engineering, University of Toronto, Toronto, Ontario M5S 3G9, Canada
[3]Developmental and Stem Cell Biology Program, The Hospital for Sick Children, Toronto, Ontario M5G 1X8, Canada

Embryonic epithelia have a remarkable ability to rapidly repair wounds. A supracellular actomyosin cable around the wound coordinates cellular movements and promotes wound closure. Actomyosin cable formation is accompanied by junctional rearrangements at the wound margin. We used in vivo time-lapse quantitative microscopy to show that clathrin, dynamin, and the ADP-ribosylation factor 6, three components of the endocytic machinery, accumulate around wounds in *Drosophila melanogaster* embryos in a process that requires calcium signaling and actomyosin contractility. Blocking endocytosis with pharmacological or genetic approaches disrupted wound repair. The defect in wound closure was accompanied by impaired removal of E-cadherin from the wound edge and defective actomyosin cable assembly. E-cadherin overexpression also resulted in reduced actin accumulation around wounds and slower wound closure. Reducing E-cadherin levels in embryos in which endocytosis was blocked rescued actin localization to the wound margin. Our results demonstrate a central role for endocytosis in wound healing and indicate that polarized E-cadherin endocytosis is necessary for actomyosin remodeling during embryonic wound repair.

Introduction

Wound repair in epithelial tissues is critical for animal survival. Epithelia line our organs and form our skin, acting as physical barriers for homeostasis and defense against pathogens. Maintenance of epithelial integrity is therefore of crucial importance and, as such, epithelial tissues can efficiently repair wounds. In particular, wound repair in the embryonic epidermis is completed rapidly, without inflammation or formation of scar tissue (Rowlatt, 1979; Harrison et al., 1990; Whitby and Ferguson, 1991).

Embryonic wound repair is driven by the assembly of a contractile "purse string" at the wound margin, a supracellular cable composed of filamentous actin and the molecular motor nonmuscle myosin II (Martin and Lewis, 1992; Brock et al., 1996). The purse string contracts (Fernandez-Gonzalez and Zallen, 2013) and coordinates the movement of the cells adjacent to the wound into the wounded region (Wood et al., 2002). The assembly of an actomyosin purse string during embryonic wound repair is conserved in a wide range of organisms both vertebrate and invertebrate, including mouse (McCluskey et al., 1993), chick (Martin and Lewis, 1992), *Xenopus laevis* (Davidson et al., 2002), and *Drosophila melanogaster* (Kiehart et al., 2000; Wood et al., 2002).

The assembly and contraction of the actomyosin purse string is accompanied by a redistribution of junctional proteins at the wound margin. In particular, the adherens junction components E-cadherin (Brock et al., 1996; Abreu-Blanco et al., 2012), α-catenin (Wood et al., 2002), and β-catenin (Zulueta-Coarasa et al., 2014) are depleted from the interfaces between wounded and adjacent cells and accumulate at discrete points at the wound margin where three cells meet. The redistribution of junctional proteins may be required for extrusion of the wounded cells. It has also been proposed that the junctional rearrangements associated with embryonic wound repair facilitate assembly and contraction of the actomyosin purse string (Brock et al., 1996; Carvalho et al., 2014).

E-cadherin down-regulation at the wound margin occurs in two sequential phases (Carvalho et al., 2014). The first phase is fast, seconds to minutes after wounding; the second phase is slow, hours after wounding. In *Drosophila* embryos, the Toll–NF-κB pathway is required for transcriptional down-regulation of E-cadherin ∼1 h after wounding (Carvalho et al., 2014). An alternative mechanism must therefore mediate the rapid initial down-regulation of E-cadherin from the wound margin. Toll–NF-κB signaling may also be important for the rapid phase by promoting changes in E-cadherin turnover. However, the mechanisms that regulate junctional turnover and the role of junctional redistribution during embryonic wound repair remain unclear.

Correspondence to Rodrigo Fernandez-Gonzalez: rodrigo.fernandez.gonzalez@utoronto.ca

Abbreviations used in this paper: ARF, ADP-ribosylation factor; dsRNA, double-stranded RNA; Rok, Rho-associated kinase; UAS, upstream activating sequence.

The Rockefeller University Press $30.00
J. Cell Biol. Vol. 210 No. 5 801–816
www.jcb.org/cgi/doi/10.1083/jcb.201501076

The endocytic machinery, used by cells to internalize molecules, can favor junctional disassembly in response to actomyosin contractility. Endocytosis has been implicated in trafficking of junctional proteins during *Drosophila* dorsal closure (Mateus et al., 2011) and zebrafish epiboly (Song et al., 2013), two processes that share several characteristics with embryonic wound repair, including epithelial sheet movements mediated by a contractile, supracellular actomyosin cable at the leading edge (Kiehart et al., 2000; Behrndt et al., 2012). Endocytosis of E-cadherin is also necessary for efficient actomyosin-mediated cell intercalation during *Drosophila* axis elongation (Levayer et al., 2011). In spite of the evidence linking actomyosin contractility, junctional disassembly, and endocytosis, the interplay between these three processes is not well understood.

In this study, we use in vivo confocal microscopy and quantitative image analysis to examine the role of endocytosis during embryonic wound repair in *Drosophila*. We find that, upon wounding, the endocytic machinery localizes to the wound margin in a calcium- and actomyosin-dependent manner. Endocytic activity is necessary for polarized E-cadherin depletion, actomyosin purse string assembly, actin-based protrusive activity, and rapid wound closure. E-cadherin overexpression recapitulates the effects of inhibiting endocytosis, and reducing E-cadherin levels when endocytosis is blocked facilitates actin remodeling around wounds. We propose that spatially regulated endocytosis orchestrates the junctional and cytoskeletal rearrangements that drive efficient wound repair.

Results

Endocytic markers accumulate at embryonic wound margins

Clathrin-mediated endocytosis has been implicated in the internalization of a wide range of cell surface and transmembrane molecules, including E-cadherin (Troyanovsky et al., 2006; Levayer et al., 2011). Clathrin-mediated endocytosis requires the vesicular coat protein, clathrin (Pearse, 1975), and the GTPase dynamin, which is necessary for scission of vesicles from the cell membrane (Damke et al., 1994). To investigate if endocytosis plays a role in embryonic wound repair, we used spinning-disk confocal microscopy and image analysis to quantify the localization of clathrin and the *Drosophila* dynamin orthologue Shibire (Chen et al., 1991) around embryonic wounds. We wounded the epidermis of *Drosophila* embryos ∼12 h after egg deposition (stage 14–15). Wounds were created by ablating two to three cells with an ultraviolet laser in embryos expressing fluorescently tagged versions of myosin, clathrin, or dynamin. Upon wounding, mean myosin fluorescence at the wound margin increased to a maximum of 2.5 ± 0.3-fold with respect to the fluorescence levels in the same region before wounding (Fig. 1, A and E; and Video 1), consistent with previous studies (Kiehart et al., 2000; Wood et al., 2002; Abreu-Blanco et al., 2012). The accumulation of myosin around the wound occurred in parallel with the reorganization of the membrane, as shown by the accumulation of myristoylated:GFP at the wound margin (Fig. S1 A). We found that GFP-fused clathrin light chain (GFP:clc) levels at the wound margin increased by 2.1 ± 0.3-fold relative to local levels before wounding (Fig. 1, B and E). Clathrin-coated vesicles accumulated in a 1.2 ± 0.1-µm-wide band around the wound (Fig. 1 B, 10 min). The accumulation of clathrin at the wound margin persisted for the duration of wound closure (Fig. 1 B and Video 2). Dynamin also accumulated at the wound margin to a maximum level of 2.0 ± 0.3-fold (Fig. 1, C and E; and Video 3). We quantified the change in total fluorescence along the perimeter of the wound and found that over time there was an increase in total protein levels for each marker, demonstrating that dynamin and clathrin accumulate at the wound margin during wound closure (Fig. 1 F). For the cells immediately adjacent to the wound, both clathrin and dynamin were enriched at plasma membranes facing the wound over those in contact with other epithelial cells (Fig. 1, B and C). Furthermore, a cytoplasmic GFP construct did not display a significant enrichment at the wound margin (Fig. S1 B), demonstrating that the accumulation of endocytic proteins around wounds is not an artifact of the loss of fluorescence inside the wound. Together, our results show a polarized accumulation of the endocytic machinery at the wound margin, suggesting that endocytosis plays a role in embryonic wound repair.

Our data indicate that the endocytic machinery is polarized upon wounding. The ADP-ribosylation factor (ARF) family of proteins, members of the Ras superfamily of small GTPases, have important roles in the regulation of endocytic trafficking (D'Souza-Schorey and Chavrier, 2006). ARF6 regulates dynamin- and clathrin-mediated endocytosis of E-cadherin from cell–cell contacts and promotes disassembly of adherens junctions (Palacios et al., 2001, 2002; Kon et al., 2008). We found that ARF6:GFP displayed a polarized distribution in the cells adjacent to the wound, accumulating at the wound margin, where ARF6 reached a maximum mean accumulation of 3.1 ± 0.5-fold (Fig. 1, D and E; and Video 4). Total ARF6 fluorescence at the wound margin increased by 2.0 ± 0.4-fold (Fig. 1 F). Thus, an endocytic regulator implicated in E-cadherin turnover becomes enriched around the wound, suggesting that E-cadherin endocytosis may be important for wound closure.

Endocytosis is necessary for rapid wound closure

To determine if endocytosis is required for efficient wound closure, we treated embryos with dynasore, a drug that blocks the ability of dynamin to hydrolyze GTP (Macia et al., 2006) and promote vesicular scission (Damke et al., 1994). Dynasore blocks all dynamin-mediated endocytosis including clathrin-mediated endocytosis (Macia et al., 2006). Immediately before wounding, we injected 50 mM dynasore into the perivitelline space of embryos expressing E-cadherin:GFP and myosin:mCherry. Wounds in dynasore-injected embryos closed at a significantly slower rate than those in control, 50% DMSO-injected embryos (0.9 ± 0.7 vs. 7.7 ± 0.9 µm²/min, respectively; $P = 5.1 \times 10^{-6}$; Fig. 2, A–D; and Video 5). Out of 11 wounds in dynasore-injected embryos, 8 wounds did not show any sign of closure within 40 min. The severe defect in wound closure after dynasore injection was not caused by dynasore-induced apoptosis, as shown by the absence of nuclear GFP in embryos expressing Apoliner, a fluorescent caspase biosensor that localizes to the nucleus upon caspase activation (Bardet et al., 2008; Fig. S2). We confirmed our dynasore results by treating embryos with 50 mM chlorpromazine, a drug that specifically blocks clathrin-mediated endocytosis (Wang et al., 1993). Perivitelline injection of chlorpromazine before wounding resulted in a significant impairment of wound closure with respect to water-injected controls (0.5 ± 0.4 vs. 18.8 ± 3.5 µm²/min, respectively; $P = 3.2 \times 10^{-3}$; Fig. S3, A–D). Together,

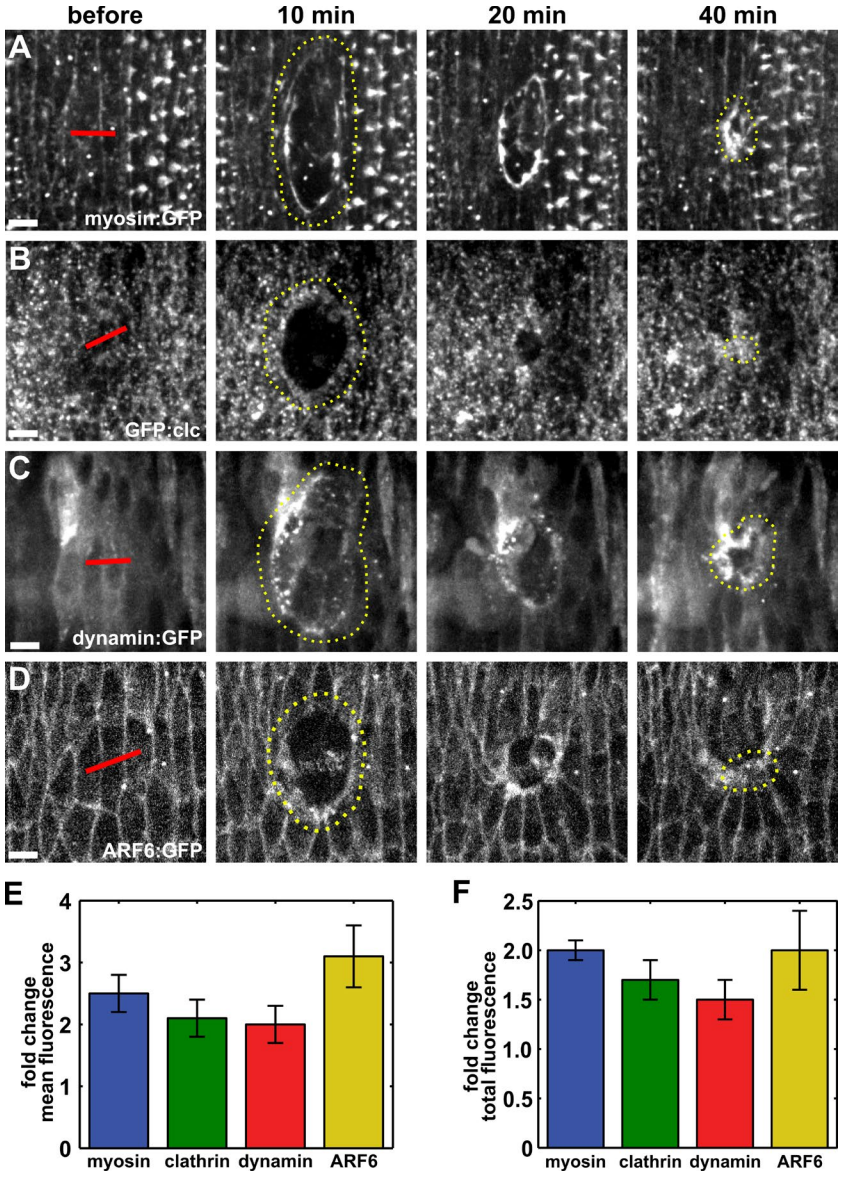

Figure 1. **Components of the endocytic machinery accumulate at the wound margin.** (A–D) Epidermal cells expressing myosin:GFP (A), GFP:clc (B), dynamin:GFP (C), or ARF6:GFP (D) in stage 14–15 embryos. Time after wounding is shown. Red lines indicate wound sites. Yellow dotted lines outline the wounds. Anterior left, dorsal up. Bars, 5 µm. (E and F) Maximum fold change in mean (E) and total (F) fluorescence of myosin:GFP (n = 6), GFP:clc (n = 5), dynamin:GFP (n = 7), and ARF6:GFP (n = 6) at the wound margin with respect to the values before wounding. Error bars denote SEM.

our pharmacological data strongly suggest that endocytosis is necessary for rapid embryonic wound repair.

To validate our pharmacological results, we took advantage of the *dynamin* temperature-sensitive mutation shi^{ts1}. When shi^{ts1} embryos are exposed to temperatures above 30°C (restrictive temperatures), the GTPase domain of dynamin undergoes a change in tertiary structure that renders it inactive (van der Bliek and Meyerowitz, 1991). At temperatures below 30°C, dynamin function is unaffected. When shi^{ts1} embryos expressing GFP:moesin, a marker of filamentous actin (Kiehart et al., 2000), were heated to the restrictive temperature immediately before wounding, the rate of wound closure was 4.0 ± 2.7 µm²/min, significantly slower than the rate of wound closure in control shi^{ts1} embryos at the permissive temperature of ~23°C (19.6 ± 4.1 µm²/min; P = 0.01; Fig. 2, F–I; and Video 6) or control GFP:moesin embryos at the restrictive temperature (21.7 ± 7.6 µm²/min; P = 0.04; Fig. 2, E and G–I; and Video 6). These results demonstrate that dynamin activity is necessary for efficient wound repair and provide further evidence indicating that endocytosis is important for embryonic wound healing.

Inhibition of endocytosis prevents cytoskeletal remodeling at the wound margin

Rapid wound closure requires the assembly of a supracellular actomyosin cable around the wound (Martin and Lewis, 1992; Brock et al., 1996; Wood et al., 2002). To establish if the delay in wound closure upon inhibition of endocytosis is associated with defects in actomyosin purse string assembly, we quantified actin and myosin dynamics at the wound margin in dynasore-treated embryos. We considered the purse string to be fully formed when either myosin or actin accumulated by 1.5-fold with respect to their values before wounding. In control embryos injected with 50% DMSO, the myosin cable was fully assembled 16.7 ± 2.7 min after wounding (Fig. 3, A and C). In contrast, in embryos in which endocytosis was blocked by injecting dynasore immediately before wounding, myosin levels around the wound did not increase significantly 40 min after wounding (Fig. 3, B and C). Overall, mean myosin fluorescence at the wound margin in dynasore-injected embryos changed by 1.2 ± 0.1-fold, a reduction of 48% with respect to controls in which myosin increased by 2.3 ± 0.3-fold (P = 5.3 × 10^{-3};

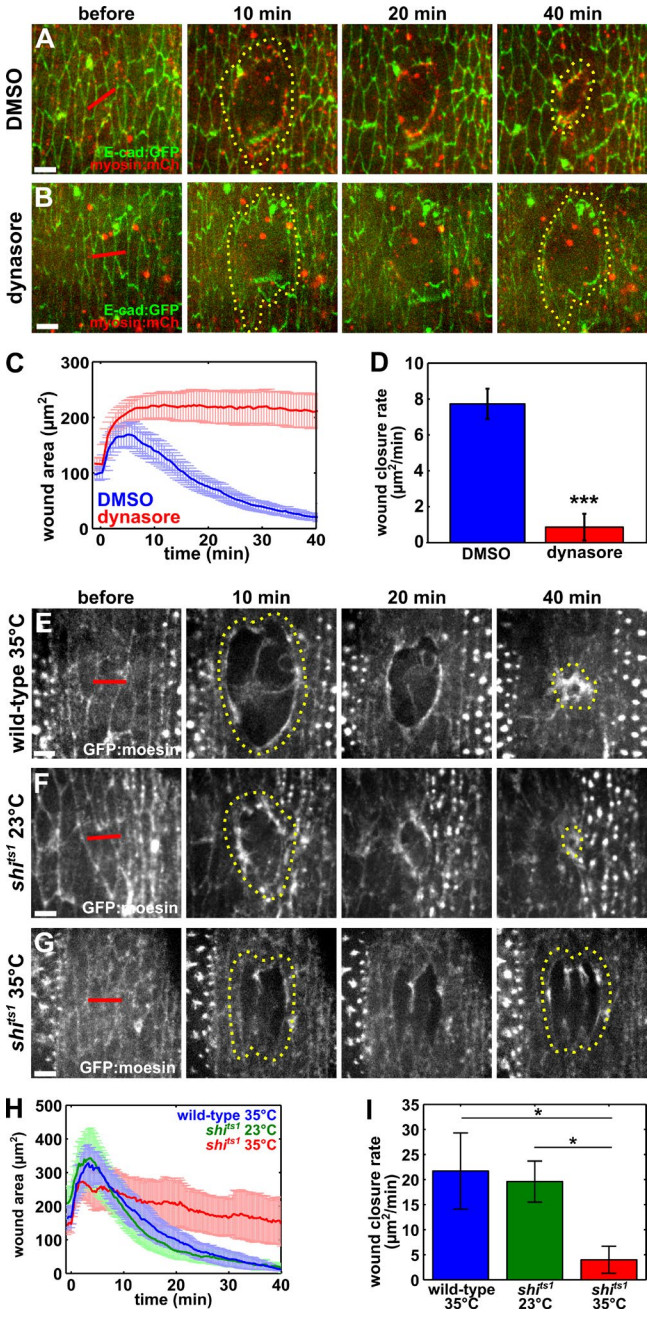

Figure 2. **Dynamin-mediated endocytosis is required for wound closure.** (A and B) Wound closure in embryos expressing E-cadherin:GFP (green) and myosin:mCherry (red), injected with DMSO (A) or dynasore (B) before wounding. (C and D) Mean wound area over time (C) and closure rate for the fast phase of wound repair (D) for control (blue; n = 12) and dynasore-injected embryos (red; n = 11). (E–G) Wound closure in wild-type embryos expressing GFP:moesin and heated to the restrictive temperature (35°C; E), or carrying a temperature-sensitive allele of dynamin (shi^{ts1}) at the permissive temperature (23°C; F) or the restrictive temperature (G). (H and I) Mean wound area over time (H) and closure rate for the fast phase of wound repair (I) for wild-type embryos at the restrictive temperature (blue; n = 5), shi^{ts1} embryos at the permissive temperature (green; n = 6), or shi^{ts1} embryos at the restrictive temperature (red; n = 6). (A, B, and E–G) Time after wounding is shown. Red lines indicate wound sites. Yellow dotted lines outline the wounds. Anterior left, dorsal up. Bars, 5 µm. Error bars, SEM; *, P < 0.05; ***, P < 0.001.

Fig. 3 D). Myosin accumulation at the wound margin was similarly impaired in shi^{ts1} embryos expressing myosin:GFP and heated to the restrictive temperature (Fig. S3, E–H).

Like myosin, F-actin did not localize to the wound margin upon blocking endocytosis. In control embryos, the actin purse string formed within 11.2 ± 4.9 min after wounding (Fig. 3, E and G). When endocytosis was blocked with dynasore, we did not measure a significant enrichment of actin around the wound 40 min after wounding (Fig. 3, F and G). The maximum actin accumulation at the wound margin when endocytosis was blocked was significantly lower than in control embryos (1.2 ± 0.1-fold vs. 2.5 ± 0.4-fold; P = 0.03; Fig. 3 H). We also quantified a significant defect in actin accumulation at the wound margin in shi^{ts1}; GFP:moesin embryos heated to the restrictive temperature (Fig. 2, F and G; and Fig. S3, I and J). Together, our results demonstrate that endocytic activity is necessary for the localization of actin and myosin to the wound margin during embryonic wound repair.

The kinase Rho-associated kinase (Rok) is one of the main activators of myosin II (Amano et al., 1996; Kimura et al., 1996), and during *Drosophila* axis elongation the recruitment of myosin to contractile supracellular cables depends on Rok (Fernandez-Gonzalez et al., 2009; Simões et al., 2010). Actin accumulation around embryonic wounds also requires the activity of Rok, which localizes to the wound margin (Verboon and Parkhurst, 2015). To determine if Rok localization to the wound margin was disrupted when we blocked endocytosis, we examined the distribution of GFP:Rok^{K116A}, a kinase-dead form of Rok previously used to measure the localization of the protein without causing phenotypes associated with excessive activation of myosin II (Simões et al., 2010), in DMSO- and dynasore-injected embryos. In DMSO-injected embryos, GFP:Rok^{K116A} accumulated at the wound margin to a maximum level of 2.6 ± 0.4-fold (Fig. 3, I, K, and L). Blocking endocytosis by injecting dynasore resulted in a maximum accumulation of GFP:Rok^{K116A} at the wound margin of 1.7 ± 0.2-fold, a significantly lower level than the controls (P = 0.04; Fig. 3, J–L). These results suggest a role for polarized endocytosis in directing the assembly of a contractile actomyosin purse string at the wound margin.

Actin-based protrusions from the cells around the wound also contribute to wound healing (Wood et al., 2002; Abreu-Blanco et al., 2012). We investigated whether protrusive activity was affected when we inhibited endocytosis. To this end, we wounded GFP:moesin embryos injected with DMSO or dynasore, and we quantified the fraction of bright pixels within a ring immediately interior to the wound margin (Zulueta-Coarasa et al., 2014). We found that protrusive activity 20 min after wounding was 53.4% lower in dynasore-injected embryos than in controls (P = 4.6×10^{-6}; Fig. 3 H, inset), suggesting that endocytosis regulates not only actomyosin purse string formation but also protrusive activity during embryonic wound repair.

Endocytosis is required for polarized removal of E-cadherin from the wound margin

Our data indicate that endocytosis is necessary for rapid wound closure. During embryonic wound repair, junctional proteins such as E-cadherin (Brock et al., 1996; Abreu-Blanco et al., 2012), α-catenin (Wood et al., 2002), and β-catenin (Zulueta-Coarasa et al., 2014) are down-regulated at the wound margin. Clathrin-mediated endocytosis has been implicated in the

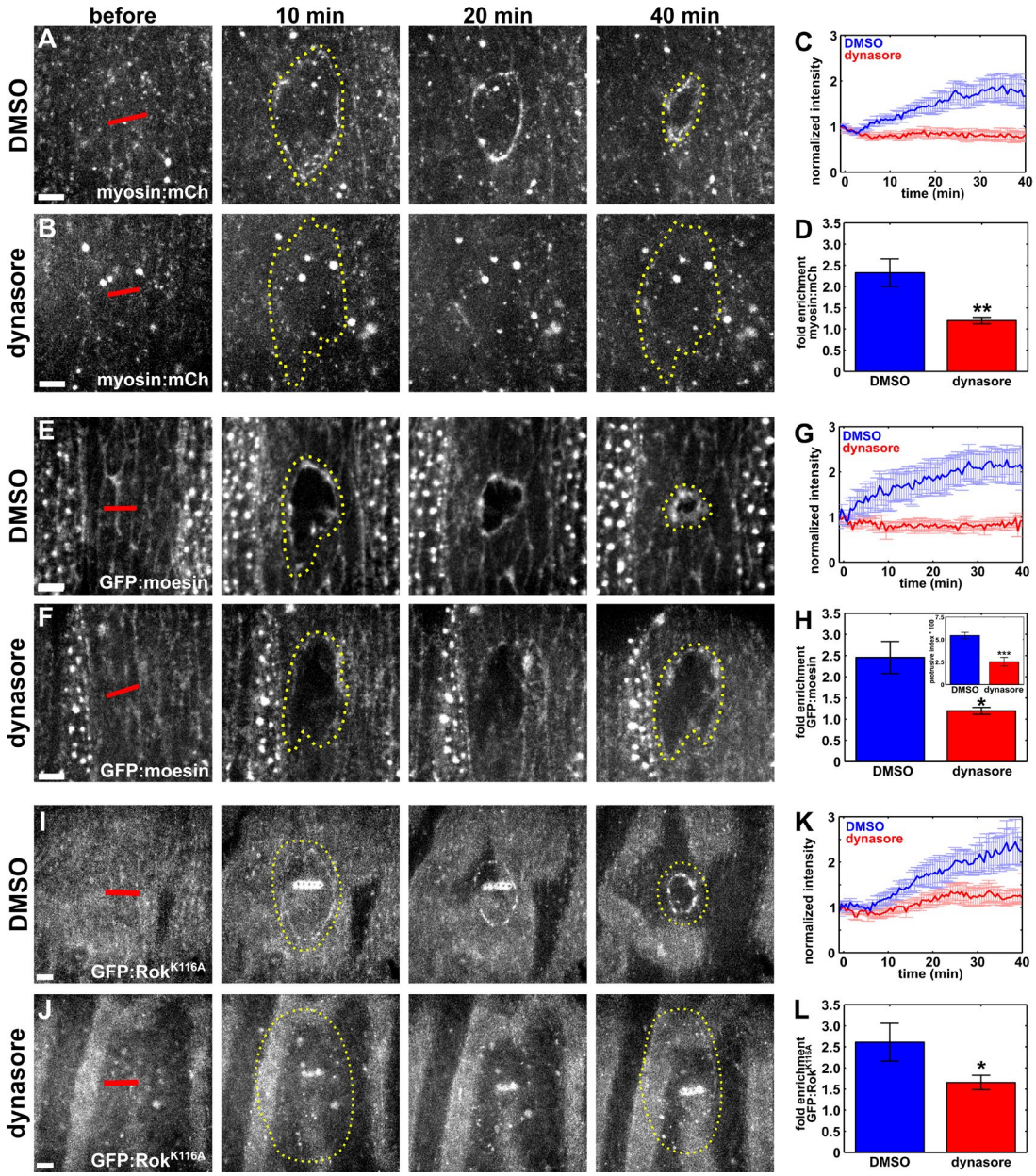

Figure 3. **Blocking endocytosis causes defective cytoskeletal remodeling during wound repair.** (A, B, E, F, I, and J) Epidermal cells expressing myosin:mCherry (A and B), GFP:moesin (E and F), or GFP:Rok^{K116A} (I and J) in embryos injected with DMSO (A, E, and I) or dynasore (B, F, and J) immediately before wounding. Time after wounding is shown. Red lines indicate wound sites. Yellow dotted lines outline the wounds. Anterior left, dorsal up. Bars, 5 µm. (C, G, and K) Mean myosin:mCherry (C), GFP:moesin (G), or GFP:Rok^{K116A} (K) fluorescence at the wound margin over time, in control, DMSO-injected embryos (blue; $n = 12$ in C, $n = 5$ in G, and $n = 6$ in K) or dynasore-injected embryos (red; $n = 11$ in C, $n = 5$ in G, and $n = 8$ in K). (D, H, and L) Maximum fold enrichment at the wound margin of myosin:mCherry (D), GFP:moesin (H), or GFP:Rok^{K116A} (L). (H, inset) Quantification of protrusive activity at the wound margin. Error bars, SEM; *, $P < 0.05$; **, $P < 0.01$; ***, $P < 0.001$.

internalization of E-cadherin from cell–cell junctions (Troyanovsky et al., 2006; Levayer et al., 2011). To determine if endocytosis is necessary for the depletion of E-cadherin from the wound margin, we used image analysis to track E-cadherin:GFP fluorescence along individual segments of the wound perimeter, both in control DMSO-injected embryos and in dynasore-treated embryos (Fig. 4, A and B, yellow boxes). In control embryos, E-cadherin:GFP fluorescence at the wound margin decreased by 40.1 ± 3.1% 15 min after wounding ($P = 5.1 \times 10^{-14}$; Fig. 4, A and C). In dynasore-treated embryos, E-cadherin:GFP fluorescence decreased only by 25.6 ± 3.0% ($P = 2.6 \times 10^{-10}$; Fig. 4, B and C). The loss of E-cadherin:GFP from the wound margin was 57% greater in controls than in dynasore-treated embryos ($P = 7.8 \times 10^{-4}$). Therefore, endocytic activity is necessary to remove E-cadherin from the interfaces between wounded and adjacent cells during the early stages of embryonic wound repair.

The asymmetric localization of the endocytic machinery in the cells adjacent to the wound suggests that E-cadherin redistribution upon wounding is polarized in these cells. To investigate if E-cadherin internalization is spatially regulated in the cells at the wound margin, we compared E-cadherin:GFP fluorescence in cell boundaries between a wounded cell and a cell adjacent to the wound (wound edges) or between two

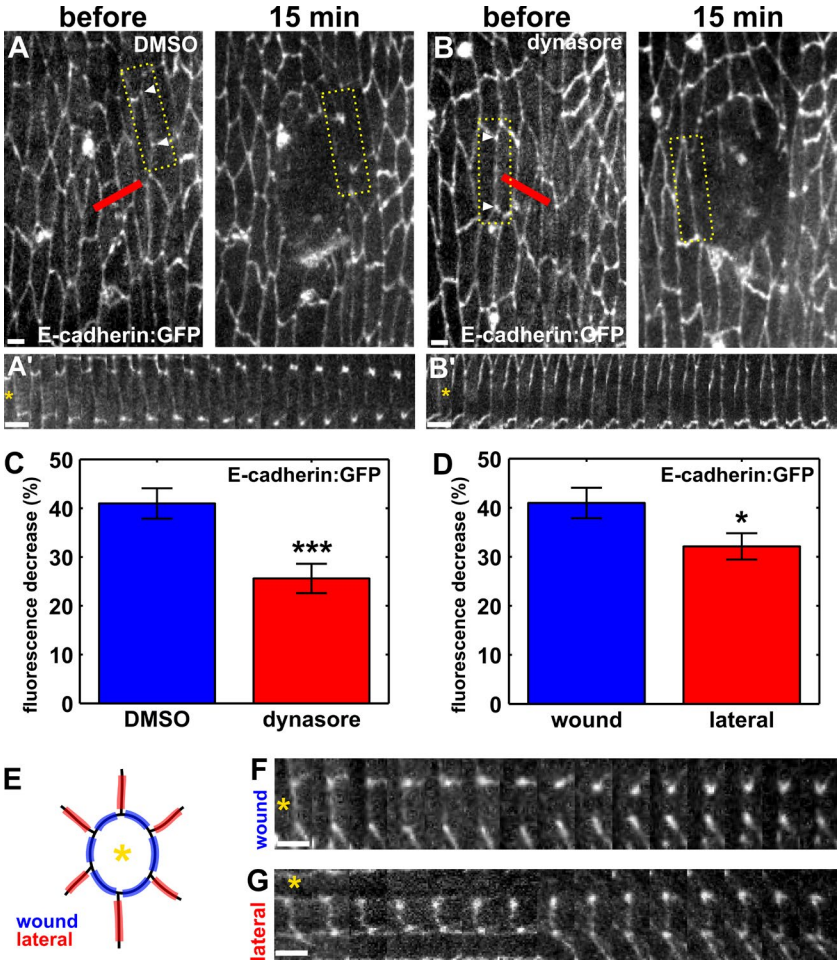

Figure 4. **Dynamin-mediated endocytosis contributes to polarized E-cadherin removal from the wound margin.** (A and B) Epidermal cells expressing E-cadherin:GFP in a DMSO-injected (A) or dynasore-injected (B) embryo. Time after wounding is shown. Red lines indicate wound sites. Arrowheads delimit boundaries used to quantify fluorescence. Yellow boxes outline the regions used to generate A′ and B′. Anterior left, dorsal up. Bars, 5 µm. (A′ and B′) Kymographs showing the redistribution of E-cadherin in the interfaces indicated in A and B. (C) Percentage of decrease in E-cadherin:GFP fluorescence at the wound margin 15 min after wounding in DMSO (n = 32 interfaces) and dynasore-injected (n = 39 interfaces) embryos. (D) Percentage of decrease in E-cadherin:GFP fluorescence 15 min after wounding in wound margin interfaces (n = 32) or lateral interfaces (n = 35). (E) Cartoon indicating the position of wound interfaces (blue, between the wound—indicated by the yellow asterisk—and an adjacent cell) and lateral interfaces (red, between two cells adjacent to the wound). (F and G) Kymographs showing E-cadherin:GFP redistribution in a wound (F) or a lateral interface (G). (A′, B′, F, and G) Asterisks denote the position of the wound. Bars, 1 min. Error bars, SEM; *, $P < 0.05$; ***, $P < 0.001$.

cells adjacent to the wound (lateral edges; Fig. 4, D–G). Mean E-cadherin:GFP fluorescence in lateral edges decreased by 32.1 ± 2.7% 15 min after wounding (Fig. 4, D and G). Thus, the reduction of E-cadherin at wound edges was significantly greater than at lateral edges ($P = 3.4 \times 10^{-2}$), suggesting that polarized E-cadherin internalization in the cells adjacent to the wound contributes to rapid embryonic wound repair.

A calcium signal and actomyosin contractility are required to polarize the endocytic machinery around wounds

What signal polarizes the endocytic machinery around embryonic wounds? Transient, large calcium stimuli promote endocytosis at nerve terminals in rat brainstems (Wu and Wu, 2014). Recent studies showed that wounding causes a transient calcium wave that decreases in amplitude as it moves away from the wound (Antunes et al., 2013; Razzell et al., 2013). Therefore, a calcium signal may promote polarized endocytosis in the cells adjacent to the wound. To investigate whether a calcium signal was implicated in the recruitment of the endocytic machinery to the wound margin, we injected embryos with 50 mM BAPTA, a cell-impermeable calcium chelator. In embryos expressing GCaMP3, a fluorescent calcium biosensor (Nakai et al., 2001; Tian et al., 2009), BAPTA injection immediately before wounding completely attenuated the calcium signal caused by wounding (Video 7). When we compared the localization of the endocytic machinery during wound repair in water or BAPTA-injected embryos, we found that in water-injected embryos dynamin:GFP accumulated at the wound margin to a maximum level of 2.5 ± 0.4-fold (Fig. 5, A, C, and D; and Video 8). In contrast, in BAPTA-treated embryos, mean dynamin fluorescence at the wound margin only increased by 1.2 ± 0.1-fold, a value 52% lower than in controls ($P = 1.6 \times 10^{-2}$; Fig. 5, B–D; and Video 8). Similarly, GFP:clc fluorescence at the wound margin in BAPTA-injected embryos displayed a maximum increase of 1.4 ± 0.1-fold, significantly lower than the 1.9 ± 0.2-fold enrichment in control embryos ($P = 1.7 \times 10^{-2}$; Fig. S4, A–D). Together, these results indicate that the polarized accumulation of the endocytic machinery to the wound margin is mediated by the release of calcium in the epidermis upon wounding, suggesting that calcium signaling may be important for cytoskeletal and junctional remodeling in embryonic wound repair.

Calcium signaling is necessary for actomyosin contractility (Hathaway and Adelstein, 1979; Scholey et al., 1980). To determine if the localization of the endocytic machinery to the wound margin required actomyosin contractility, we injected embryos with 10 mM Y-27632, a Rok inhibitor. Rok inhibition blocks actomyosin contractility during embryonic development in *Drosophila* (Fernandez-Gonzalez et al., 2009). In embryos expressing dynamin:GFP and injected with Y-27632, dynamin reached a maximum accumulation at the wound margin of 1.3 ± 0.1-fold, 28% lower than the 1.8 ± 0.01-fold accumulation in control embryos ($P = 9.6 \times 10^{-3}$; Fig. 5, E–H). Clathrin recruitment to the wound margin was similarly impaired upon blocking actomyosin contractility: GFP:clc accumulated to a maximum level of 1.2 ± 0.1-fold in Y-27632–treated embryos,

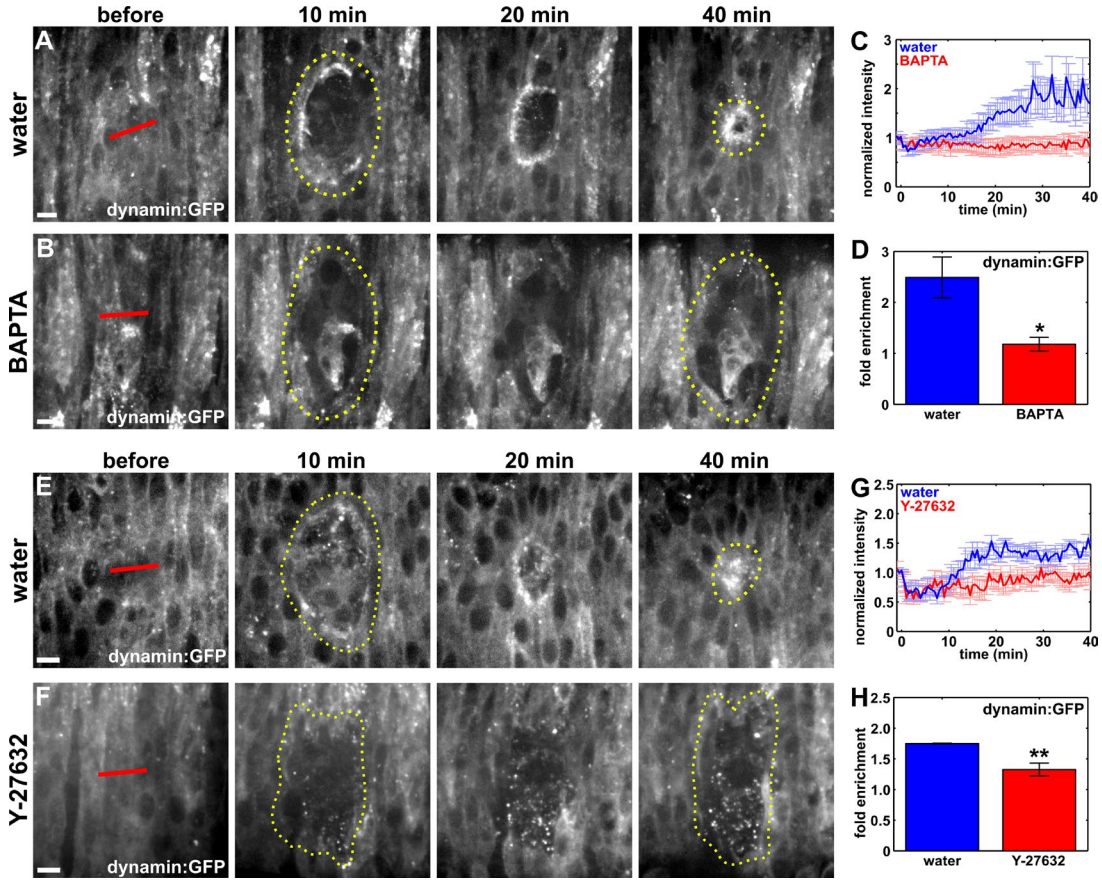

Figure 5. **Calcium and actomyosin contractility are required for the recruitment of dynamin to the wound.** (A, B, E, and F) Epidermal cells in embryos expressing dynamin:GFP, injected with water (A and E), BAPTA (B), or Y-27632 (F). Time after wounding is shown. Red lines indicate wound sites. Yellow dotted lines outline the wounds. Anterior left, dorsal up. Bars, 5 µm. (C and G) Dynamin:GFP fluorescence at the wound margin over time, in water (blue; $n = 7$ in C and $n = 5$ in G), BAPTA (red; $n = 6$ in C), or Y-27632 (red; $n = 6$ in G)–injected embryos. (D and H) Maximum fold enrichment of dynamin:GFP at the wound margin. Error bars, SEM; *, $P < 0.05$; **, $P < 0.05$.

43% lower than the 2.1 ± 0.1-fold accumulation we quantified in water-injected controls ($P = 1.1 \times 10^{-3}$; Fig. S4, E–H). Together, these results indicate that actomyosin contractility is required for the polarized accumulation of the endocytic machinery at the periphery of the wound.

Calcium signaling is necessary for rapid wound closure, purse string formation, and E-cadherin redistribution

Our results showing that calcium is necessary for the polarization of the endocytic machinery to the wound margin predict that blocking calcium signaling should cause phenotypes similar to those resulting from blocking endocytosis. To investigate whether wound healing was delayed when we blocked calcium release, we measured the rate of wound closure in BAPTA-treated embryos (Fig. 6, A–D). Blocking calcium release led to wounds that closed at a rate of 11.9 ± 2.4 µm²/min, significantly slower than wounds in water-injected controls, which closed at a rate of 20.2 ± 3.4 µm²/min ($P = 3.8 \times 10^{-2}$; Fig. 6 D). We confirmed these results by treating embryos with 500 µM thapsigargin, a cell-permeable calcium chelator, which also delayed wound healing (Fig. S4, I and J). These data show that calcium release is necessary for rapid wound repair.

In the *Drosophila* pupal notum, calcium release upon wounding is necessary for actomyosin purse string formation (Antunes et al., 2013). However, the mechanisms by which calcium mediates purse string assembly remain unclear. We examined whether calcium is required for purse string formation in the embryonic epidermis by quantifying actin intensity at the wound margin in BAPTA-treated embryos expressing mCherry:moesin. When we blocked calcium signaling, actin fluorescence at the wound margin reached a maximum level of 1.6 ± 0.2-fold, significantly lower than the 2.5 ± 0.2-fold increase in actin intensity in control, water-injected embryos (56% reduction; $P = 7.5 \times 10^{-3}$; Fig. 6, E–H).

To determine if the defect in purse string formation when we blocked calcium release was associated with increased E-cadherin at the wound margin, we quantified E-cadherin:GFP fluorescence around wounds in BAPTA-treated embryos. Calcium binds to cadherins to prevent their degradation (Yoshida and Takeichi, 1982) and, thus, BAPTA treatment could impair cell–cell adhesion. In spite of this, we quantified significantly higher levels of E-cadherin at the wound margin in BAPTA-injected embryos. In water-injected controls, E-cadherin:GFP fluorescence decreased by 36.9 ± 5.4% 15 min after wounding ($P = 8.9 \times 10^{-7}$; Fig. 6, I and K; and Video 9). In contrast, in BAPTA-treated embryos there was not a significant reduction in E-cadherin:GFP fluorescence at the wound margin within 15 min (2.0 ± 9.0%; $P = 0.82$; Fig. 6, J and K; and Video 9). The depletion of E-cadherin from the wound margin was therefore significantly higher in controls than in BAPTA-injected embryos ($P = 2.1 \times 10^{-3}$; Fig. 6 K). Similarly, E-cadherin levels

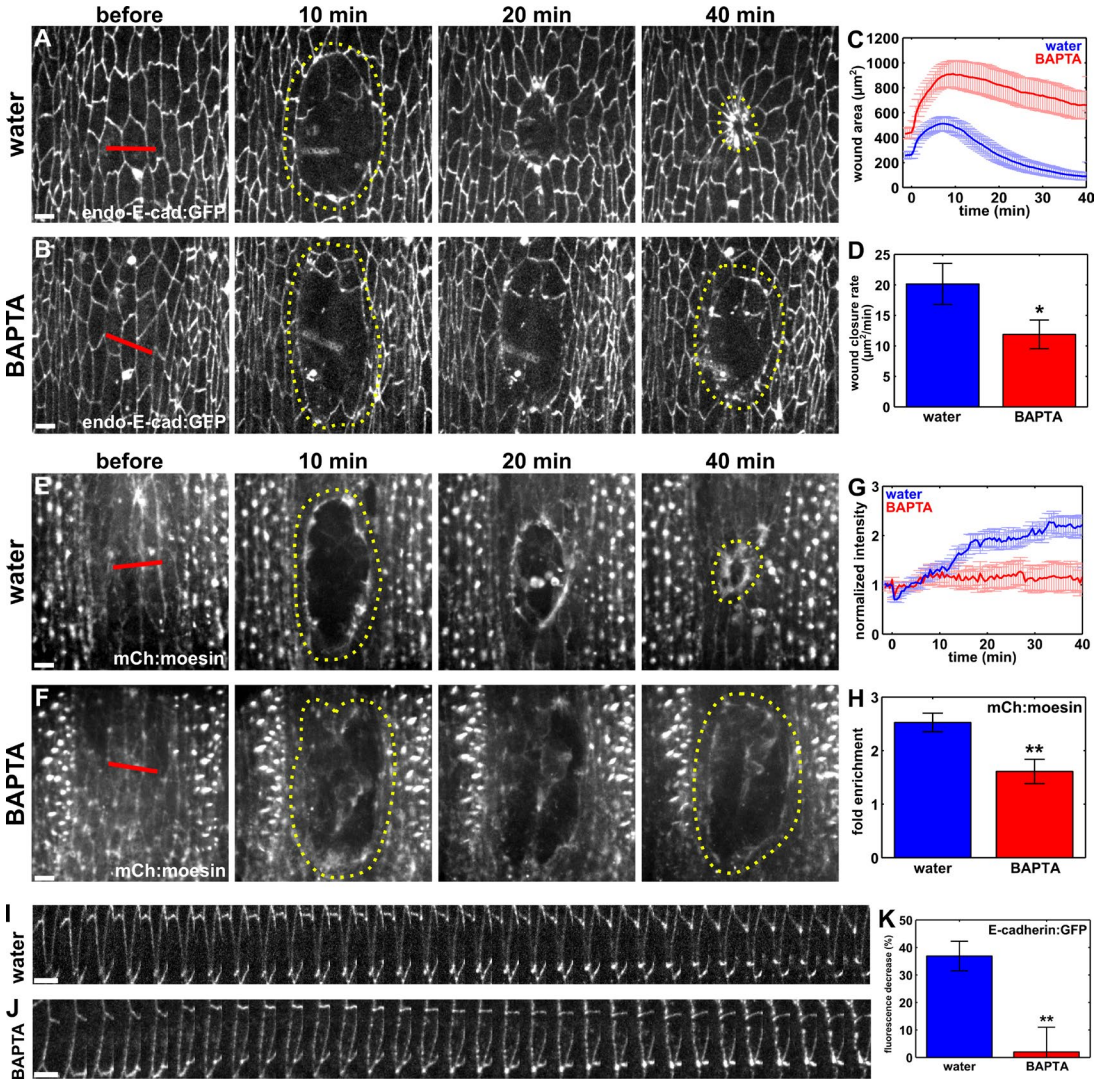

Figure 6. **Calcium is required for E-cadherin redistribution at the wound margin, purse string formation, and rapid wound repair.** (A, B, E, and F) Epidermal cells in embryos expressing endo–E-cadherin:GFP (A and B) or mCherry:moesin (E and F), injected with water (A and E) or BAPTA (B and F) before wounding. Bars, 5 µm. (C and G) Wound area over time for water-injected (blue; $n = 8$ in C and $n = 7$ in G) and BAPTA-injected (red; $n = 10$ in C and $n = 7$ in G) embryos. (D) Wound closure rate for the fast phase of tissue repair. (H) Maximum fold enrichment of mCherry:moesin at the wound margin. (I and J) Kymographs showing E-cadherin:GFP redistribution along cell interfaces at the wound margin. Anterior left, dorsal up. Bars, 30 s. (K) Percentage of decrease in E-cadherin:GFP fluorescence along wound margin interfaces 15 min after wounding in water-injected ($n = 22$ interfaces) and BAPTA-injected ($n = 21$ interfaces) embryos. (A–D) Time after wounding is shown. Red lines indicate wound sites. Yellow dotted lines outline the wounds. Anterior left, dorsal up. Error bars, SEM; *, $P < 0.05$; **, $P < 0.01$.

at the wound margin 15 min after wounding were significantly higher in thapsigargin-treated embryos in comparison to DMSO-injected controls ($P = 5.5 \times 10^{-3}$; Fig. S4, I′, J′, and K). Therefore, a calcium signal is necessary for the polarized removal of E-cadherin from the wound margin. Together, our results strongly suggest that the release of calcium in the embryonic epidermis upon wounding triggers the accumulation of the endocytic machinery at the wound margin and that polarized endocytosis of E-cadherin from the interfaces between wounded and adjacent cells is required for actomyosin purse string formation and rapid wound closure.

E-cadherin overexpression delays wound closure and impairs cytoskeletal rearrangements

Our results suggest that E-cadherin endocytosis is required for rapid wound repair. To investigate if E-cadherin specifically needs to be removed from the wound margin, we overexpressed E-cadherin in the embryonic epidermis using the upstream activating sequence (UAS)–Gal4 system (Brand and Perrimon, 1993) and the strong driver *tubulin*-Gal4, which is expressed in every cell at every stage of development (Lee and Luo, 1999). We quantified wound-closure rates in embryos overexpressing UAS–E-cadherin:GFP and found that wound repair proceeded at a significantly slower rate (17.5 ± 1.4 µm²/min) than in embryos expressing wild-type levels of E-cadherin (34.4 ± 4.0 µm²/min; $P = 4.5 \times 10^{-3}$; Fig. 7, A–C). Notably, when we quantified the rate of wound closure in embryos expressing E-cadherin:GFP at endogenous levels (endo–E-cadherin:GFP; Huang et al., 2009), mildly increased levels (ubi–E-cadherin:GFP; Oda and Tsukita, 2001), or high levels (UAS–E-cadherin:GFP), we found that slower wound closure correlated with increasing E-cadherin expression (Fig. 7, D and E). To further test if increasing E-cadherin levels disrupted wound closure, we

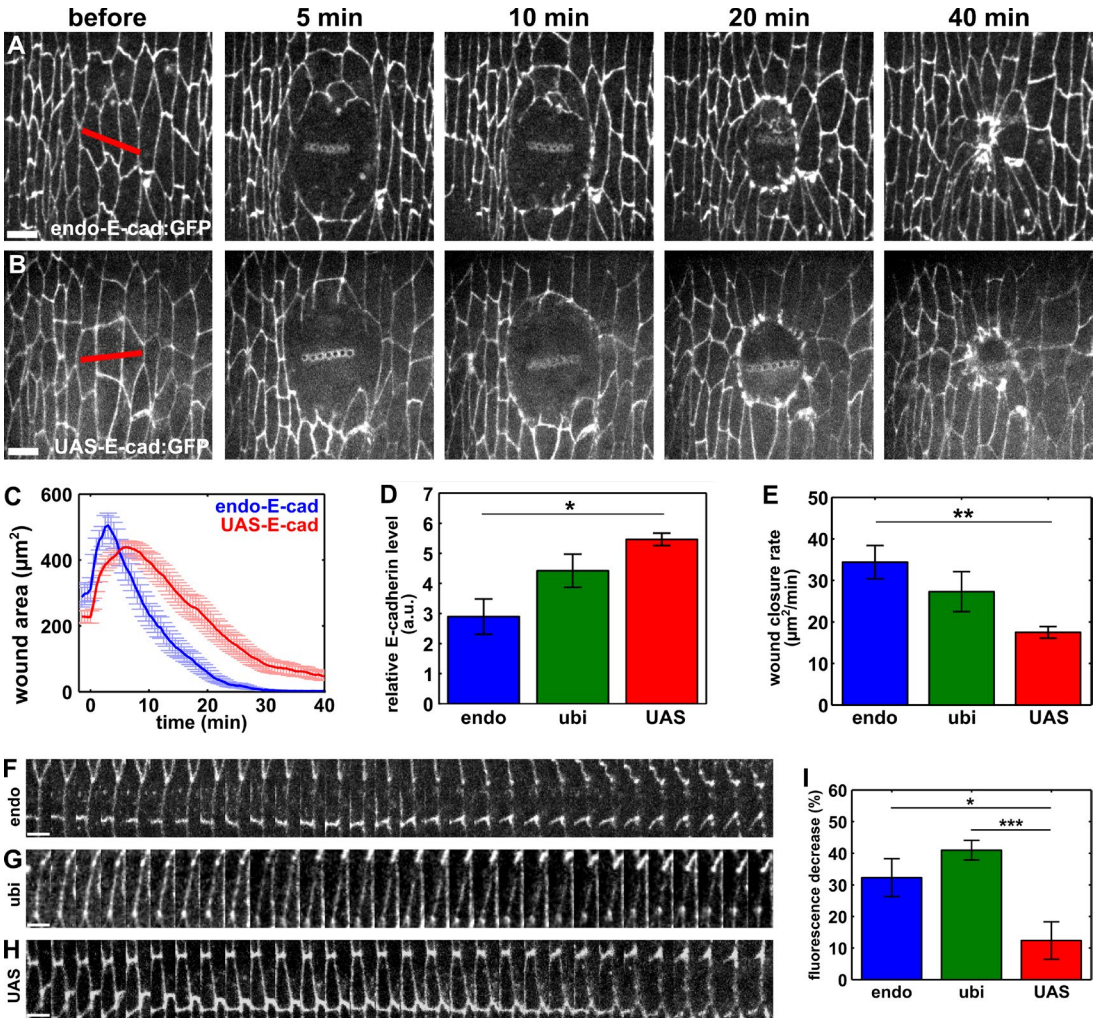

Figure 7. **E-cadherin overexpression delays wound closure.** (A and B) Epidermal cells in embryos expressing wild-type levels of E-cadherin (endo–E-cad:GFP) or overexpressing E-cadherin (UAS–E-cad:GFP). Time after wounding is shown. Red lines indicate wound sites. Anterior left, dorsal up. Bars, 5 µm. (C) Mean wound area over time in embryos expressing wild-type levels of E-cadherin (blue; $n = 7$) or overexpressing E-cadherin (red; $n = 8$). (D and E) Relative E-cadherin fluorescence in cell interfaces with respect to the counterstain (Dlg; D) and wound closure rate for the fast phase of wound repair (E) in stage 14–15 embryos expressing endo–E-cadherin:GFP (endo; $n = 5$), ubi–E-cadherin:GFP (ubi; $n = 5$), or UAS–E-cadherin:GFP driven by *tubulin-Gal4* (UAS; $n = 5$). (F–H) Kymographs showing the redistribution of E-cadherin:GFP along cell interfaces at the wound margin in embryos expressing endo–E-cadherin:GFP (F), ubi–E-cadherin:GFP (G), or UAS–E-cadherin:GFP (H). Anterior left, dorsal up. Bars, 30 s. (I) Percentage of decrease in E-cadherin:GFP fluorescence from interfaces at the wound margin 15 min after wounding in embryos expressing endo–E-cadherin:GFP ($n = 23$ interfaces), ubi–E-cadherin:GFP ($n = 32$ interfaces), and UAS–E-cadherin:GFP ($n = 20$ interfaces). Error bars, SEM; *, $P < 0.05$; **, $P < 0.01$; ***, $P < 0.001$.

overexpressed p120-catenin using *tubulin*-Gal4. p120-catenin stabilizes E-cadherin at adherens junctions by preventing its endocytosis (Ishiyama et al., 2010; Nanes et al., 2012). Overexpression of p120-catenin resulted in significantly higher levels of junctional E-cadherin (61.7% increase; $P = 0.02$; Fig. S5 E). When we overexpressed p120-catenin, the rate of wound closure decreased significantly, from 34.4 ± 4.0 µm²/min in controls to 18.7 ± 5.1 µm²/min in p120-catenin–overexpressing embryos ($P = 0.03$; Fig. S5, A–D). Together, our data suggest that E-cadherin levels must be tightly regulated to promote rapid embryonic wound repair.

To determine whether E-cadherin overexpression affects the redistribution of junctional proteins during wound repair, we quantified E-cadherin:GFP fluorescence at the wound margin in embryos expressing E-cadherin:GFP from the endogenous E-cadherin promoter and in embryos in which E-cadherin:GFP was overexpressed using the UAS-Gal4 system. In embryos expressing endo–E-cadherin:GFP, we found a 32.3 ± 6.0% reduction in E-cadherin fluorescence from interfaces between wounded and adjacent cells 15 min after wounding ($P = 1.9 \times 10^{-5}$; Fig. 7, F and H). In contrast, in embryos overexpressing UAS–E-cadherin:GFP, fluorescence only decreased by 12.4 ± 5.9% during the same time period ($P = 0.05$; Fig. 7, H and I). The loss of E-cadherin:GFP from the wound margin was 160% greater in endo–E-cadherin:GFP embryos than in embryos overexpressing UAS–E-cadherin:GFP ($P = 2.3 \times 10^{-2}$; Fig. 7 I). We also quantified significantly lower levels of E-cadherin:GFP at the wound margin in embryos expressing ubi–E-cadherin:GFP in comparison to those overexpressing UAS–E-cadherin:GFP ($P = 1.7 \times 10^{-4}$; Fig. 7, G–I). Our data show that overexpression of E-cadherin results in higher E-cadherin levels at the interfaces between wounded and adjacent cells, thus affecting the normal redistribution of junctional proteins associated with wound repair.

Blocking endocytosis resulted in significantly higher levels of E-cadherin at the wound margin (Fig. 4) accompa-

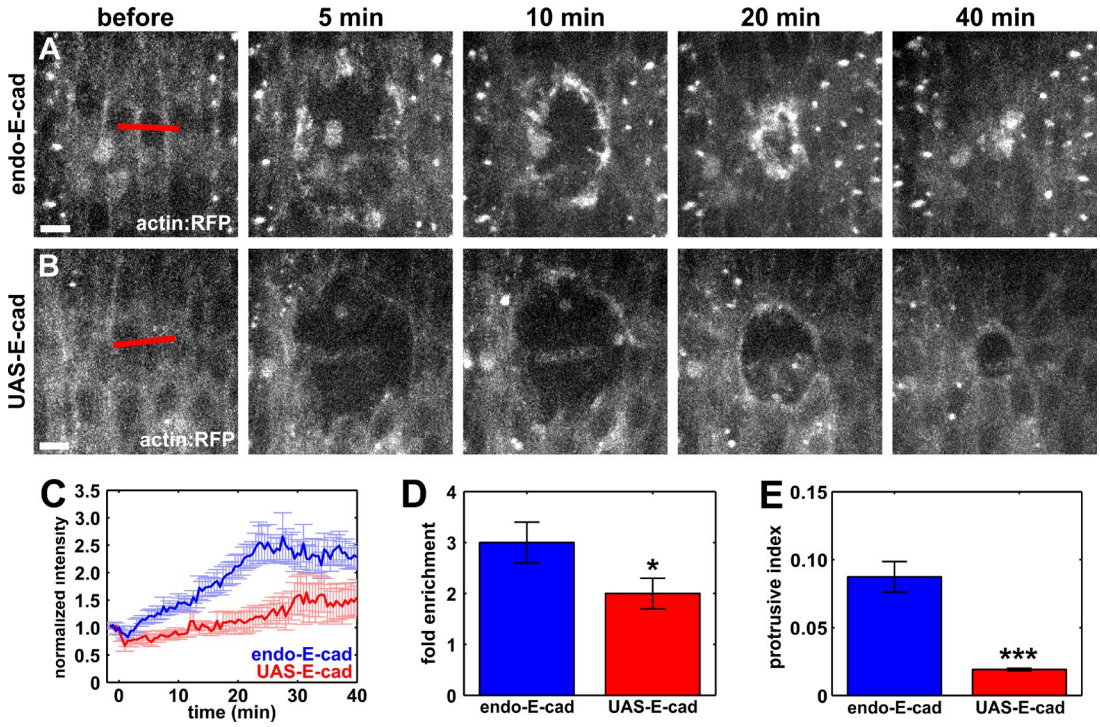

Figure 8. **E-cadherin overexpression causes defects in actin dynamics at the wound margin.** (A and B) Epidermal cells in embryos expressing actin:RFP (A and B) and E-cadherin at wild-type levels (A) or overexpressing E-cadherin:GFP (B). Time after wounding is shown. Red lines indicate wound sites. Anterior left, dorsal up. Bars, 5 µm. (C) Actin:RFP fluorescence at the wound margin in embryos expressing wild-type levels of E-cadherin (blue; $n = 7$) or overexpressing E-cadherin:GFP (red; $n = 8$). (D) Maximum fold enrichment of actin:RFP at the wound margin. (E) Quantification of protrusive activity at the wound margin. Error bars, SEM; *, $P < 0.05$; ***, $P < 0.001$.

nied by a significant reduction in F-actin, myosin II, and Rok (Fig. 3). Therefore, we predicted that purse string assembly would be disrupted in embryos overexpressing E-cadherin. To determine whether overexpression of E-cadherin affected purse string formation, we quantified actin:RFP fluorescence at the wound margin in embryos expressing wild-type levels of E-cadherin and in embryos overexpressing E-cadherin:GFP. In embryos overexpressing E-cadherin, actin:RFP reached a maximum accumulation of 2.0 ± 0.3-fold around the wound, significantly lower than the 3.0 ± 0.4-fold enrichment in actin:RFP fluorescence at the wound margin in control embryos ($P = 0.04$; Fig. 8, A–D). These results indicate that E-cadherin depletion from the wound margin is required for the accumulation of actin around the wound. We also found a significant reduction in protrusive activity at the wound margin in embryos overexpressing E-cadherin ($P = 3.9 \times 10^{-7}$; Fig. 8 E), further indicating that excess E-cadherin at the wound margin impairs the cytoskeletal rearrangements associated with wound closure. Together, our data strongly suggest that polarized E-cadherin endocytosis in the cells adjacent to the wound is required for the assembly of the cytoskeletal structures that mediate force generation and coordinate cell movement to promote rapid embryonic wound repair.

E-cadherin reduction partially rescues purse string formation and protrusive activity when endocytosis is blocked

If endocytosis of E-cadherin is specifically required for actin accumulation around embryonic wounds, decreasing E-cadherin levels in embryos in which endocytosis was blocked should facilitate actin assembly at the wound margin. To reduce E-cadherin levels, we injected syncytial embryos with double-stranded RNA (dsRNA) against *shotgun* (*shg*, *Drosophila* E-cadherin) at 27.5 ng/µl. dsRNA treatment reduced E-cadherin in the epidermis of embryos at the permissive temperature to 58% of the levels in water-treated controls ($P = 0.01$; Fig. 9, A–C). Partial rather than complete E-cadherin depletion was necessary to allow embryos to develop to stage 14. The reduction in E-cadherin levels did not rescue the wound closure phenotype caused by blocking dynamin in shi^{ts1}; GFP:moesin embryos at the restrictive temperature (Fig. 9, D–F). However, E-cadherin reduction in shi^{ts1} embryos at the restrictive temperature resulted in the presence of actin-rich segments and protrusions at the wound margin (Fig. 9, E, G, and H). To quantify the presence of actin-rich structures, we measured the 90th percentile of the actin signal in the pixels around the wound. We found that, in shi^{ts1} embryos injected with *shg* dsRNA and heated to the restrictive temperature, the maximum level of actin at the wound margin increased by 12.5 ± 4.4% at 39.5 min after wounding. This was a significantly greater change than the 3.4 ± 2.2% maximum increment found 20 min after wounding in water-injected shi^{ts1} embryos at the restrictive temperature ($P = 0.05$; Fig. 9 G). Protrusive activity increased by 145% when we reduced E-cadherin levels in embryos in which endocytosis was blocked ($P = 1.2 \times 10^{-12}$; Fig. 9 H). Together, our data indicate that decreasing E-cadherin levels when endocytosis is blocked facilitates actin accumulation and protrusive activity around embryonic wounds, providing further evidence to suggest that endocytosis contributes to wound repair at least in part by removing E-cadherin from the wound margin to facilitate cytoskeletal rearrangements.

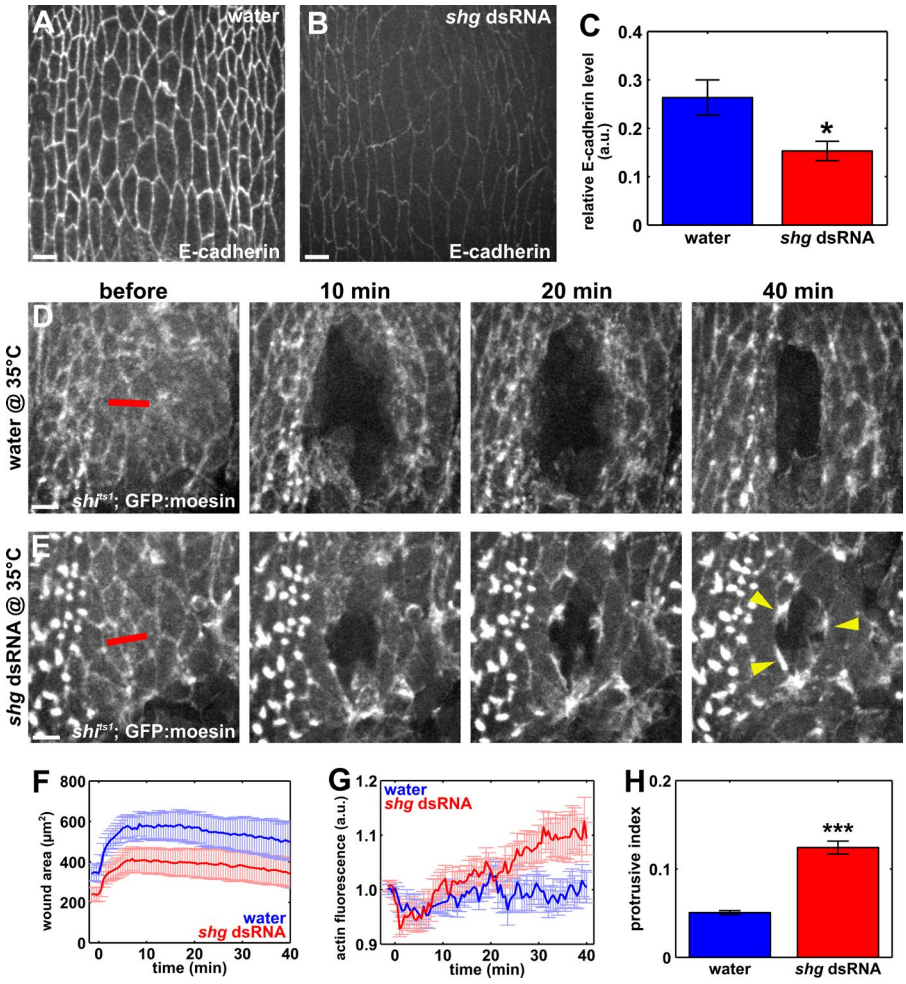

Figure 9. **E-cadherin down-regulation partially rescues purse string formation when endocytosis is blocked.** (A and B) Epidermal cells in embryos injected with water (A) or *shg* dsRNA (B) and immunostained for E-cadherin. (C) Relative junctional E-cadherin fluorescence with respect to the counterstain (Dlg) in *yellow white* embryos injected with water (blue; n = 7) or 27.5 ng/μl *shg* dsRNA (red; n = 10). (D and E) Epidermal cells in shi^{ts1}; GFP:moesin embryos at the restrictive temperature (35°C), injected with water (D) or *shg* dsRNA (E). Time after wounding is indicated. Red lines represent wound sites. Yellow arrowheads point at actin-rich regions at the wound margin. (A, B, D, and E) Anterior left, dorsal up. Bars, 5 μm. (F) Mean wound area in shi^{ts1} embryos at the restrictive temperature, injected with water (blue; n = 9) or *shg* dsRNA (red; n = 11). (G) Quantification of actin-rich structures at the wound margin, represented as the 90th percentile of the actin fluorescence around the wound. (H) Quantification of protrusive activity at the wound margin. Error bars, SEM; *, $P < 0.05$; ***, $P < 0.001$.

Discussion

An outstanding question in cell and developmental biology is how cells coordinate their movements. Using quantitative imaging and pharmacological and genetic manipulations, we demonstrate that endocytosis is essential for collective cell migration during *Drosophila* embryonic wound repair. Inhibition of endocytosis disrupts junctional remodeling, prevents the assembly of the supracellular actomyosin cable that coordinates cell migration, and dramatically slows down wound closure. Overexpression of E-cadherin, a core junctional component, phenocopies inhibition of endocytosis, and partial depletion of E-cadherin when endocytosis is blocked rescues actin assembly around wounds, suggesting that E-cadherin endocytosis is a necessary step for the cytoskeletal rearrangements associated with embryonic wound repair.

We show that the endocytic machinery is deployed to the wound margin within minutes, in a process that requires actomyosin contractility. Actomyosin contractility is necessary for polarized clathrin accumulation at the rear end of migrating T cells (Samaniego et al., 2007), and it has been proposed that actomyosin assembly and contraction induce spatially regulated E-cadherin clustering and polarized membrane recruitment of the endocytic machinery during *Drosophila* axis elongation (Levayer et al., 2011). What are the contractile forces that promote the localization of the endocytic machinery to the wound margin? Polarized endocytosis is required for purse string assembly, suggesting that purse string contraction does not trigger the polarization of clathrin and dynamin. Epidermal cells display myosin pulses on their medial-apical cortex (Fernandez-Gonzalez and Zallen, 2013) that could contribute to the localization of the endocytic machinery to the wound edge. Further experiments locally manipulating myosin activity in different subcellular domains (Morckel et al., 2012) will help to clarify the complex interplay between the cytoskeleton and endocytosis during wound repair.

Our data show that a calcium signal promotes the polarized recruitment of the molecules necessary for endocytosis to the wound margin. Mechanically gated ion channels are activated upon wounding (Xu and Chisholm, 2011; Antunes et al., 2013) and could enable calcium entry into the cells adjacent to the wound, actomyosin contractility, and localization of the endocytic machinery to the wound margin. Calcium could also promote polarized endocytosis through other mechanisms. Calcium entry into single cells upon wounding promotes membrane resealing (Steinhardt et al., 1994), and this reorganization of the membrane could facilitate the accumulation of membrane-associated endocytic molecules. Calcium triggers calcineurin-mediated dephosphorylation of dynamin II, the mammalian orthologue of *Drosophila* Shibire, during cytokinesis (Chircop et al., 2010). Dynamin II dephosphorylation is necessary for its localization to the midbody and the completion of cell division (Chircop et al., 2011). Calcium binding also promotes recruitment of the clathrin light chain (Mooibroek et al., 1987) and assembly of clathrin

coats (Keen et al., 1979). Therefore, calcium entry into the cells adjacent to the wound could directly and indirectly control the recruitment of the endocytic machinery to the wound margin.

Our data strongly suggest that E-cadherin endocytosis regulates actomyosin network assembly in vivo. Endocytosis may redistribute E-cadherin and other junctional proteins to discrete points at the wound margin where they can initiate actin polymerization (Ratheesh and Yap, 2012) and provide anchor points for the assembly of the purse string (Brock et al., 1996). E-cadherin internalization may also destabilize the bonds between α-catenin and the cytoskeleton, thus facilitating disassembly of the apical, actin-rich cortex to provide short actin filaments that act as a substrate for Arp2/3-mediated actin polymerization at the wound edge (Campos et al., 2010; Suraneni et al., 2012; Chen and Pollard, 2013; Kumar et al., 2015) or protrusive activity driven by Diaphanous and/or Ena/VASP (Homem and Peifer, 2009). A dileucine motif in the juxtamembrane domain of E-cadherin regulates its endocytosis (Miyashita and Ozawa, 2007); however, this motif is not conserved in *Drosophila* (Nanes et al., 2012). Experiments using forms of E-cadherin that cannot be endocytosed will contribute to clarifying the relationship between junctional redistribution and cytoskeletal dynamics during wound healing in vivo.

The interaction of endocytic molecules with the cytoskeleton could directly regulate actomyosin remodeling at the wound margin. Dynamin has a putative actin-binding domain that can induce actin polymerization by displacing capping proteins such as gelsolin (Gu et al., 2010). In mammalian cells, dynamin can interact with Rok (Tumusiime et al., 2009), a regulator of actin dynamics (Mason et al., 2013) and one of the main activators of myosin II (Amano et al., 1996; Kimura et al., 1996). Mutating dynamin has a similar effect on cytoskeletal organization as Rok inhibition, and expression of dominant-negative dynamin can be rescued by coexpression of constitutively active Rok, suggesting that dynamin may directly regulate Rok (Tumusiime et al., 2009). Consistent with this, we find that the accumulation of Rok at the wound edge is strongly reduced when dynamin activity is inhibited. Dynasore treatment and the shi^{ts1} mutation used in our study affect the GTPase domain of dynamin, suggesting that it is the role of dynamin in vesicle scission that is important for actomyosin purse string assembly. However, the GTPase domain of dynamin has also been implicated in cytoskeletal remodeling (Schafer et al., 2002), and therefore, we cannot exclude the possibility that dynamin directly regulates actomyosin dynamics during embryonic wound closure.

Endocytosis may regulate other molecules in addition to E-cadherin during wound repair. Integrins have been implicated in embryonic wound closure (Campos et al., 2010), are regulated via endocytosis (Caswell et al., 2009), and can sequester actin filaments similar to adherens junctions. Members of the PAR polarity complex are also trafficked via endocytosis (Nakayama et al., 2009); and Bazooka/Par-3 specifically is depleted from embryonic wound margins (Pickering et al., 2013) in a process that restricts the localization of the lipid phosphatase PTEN, thus driving PIP3 accumulation around the wound and protrusive activity. Importantly, overexpression of PTEN inhibits actin-based protrusions at wound edges, but not the assembly of the actin purse string (Pickering et al., 2013), suggesting that if Bazooka/Par-3 is regulated by endocytosis during wound repair, this process may not be necessary for purse string formation.

The assembly of supracellular actomyosin networks is a conserved feature of collective cell behavior in development and disease. Therefore, the relationship that we found between E-cadherin dynamics, actomyosin network formation, and collective cell migration may be at play in other systems. For instance, metastatic cells down-regulate E-cadherin both transcriptionally (Lombaerts et al., 2006) and through endocytosis and degradation (Yang et al., 2006). It has been proposed that the down-regulation of E-cadherin in metastatic cells facilitates detachment from their neighbors and invasion. In addition, metastatic cells can migrate as small clusters (Yamamoto et al., 1983; DiCostanzo et al., 1990) in which individual cell movements are coordinated by the assembly of a supracellular actomyosin cable around the cluster (Gaggioli et al., 2007; Hidalgo-Carcedo et al., 2011). An interesting possibility is that the down-regulation of E-cadherin in metastatic cells is a prerequisite for the assembly of the supracellular actomyosin cable that coordinates cluster migration. Consistent with this, blocking endocytosis in metastatic cells decreases the efficiency of their migration (Eppinga et al., 2012). Further experiments using metastatic cell lines and animal models of metastasis will help to determine the interactions between E-cadherin, trafficking, and actomyosin dynamics in abnormal invasive behaviors.

Materials and methods

Fly stocks

The following markers were used for live imaging: *endo-DE-cadherin:GFP* (Huang et al., 2009), *ubi-DE-cadherin:GFP* (Oda and Tsukita, 2001), *UAS-DE-cadherin:GFP* (gift of N. Gorfinkiel, Consejo Superior de Investigaciones Cientificas–Universidad Autónoma de Madrid, Madrid, Spain), *UAS-p120-catenin:GFP* (Bloomington Drosophila Stock Center; Myster et al., 2003), *UAS-actin:RFP* (Simões et al., 2006; gift of N. Gorfinkiel), *sqh-GFP:moesin* (Kiehart et al., 2000), *UAS-mCherry:moesin* (Millard and Martin, 2008), *sqh-sqh:GFP* (Royou et al., 2004), *sqh-sqh:mCherry* (Martin et al., 2009), *sqh-GFP:*rok^{K116A} (Simões et al., 2010), *UAS-GFP:clc* (Chang et al., 2002), *20XUAS-*shi^{ts1}*:GFP* (Pfeiffer et al., 2012), *UAS-Apoliner* (Bloomington Drosophila Stock Center; Bardet et al., 2008), *UAS-GFP* (gift of U. Tepass, University of Toronto, Toronto, Canada), *10XUAS-myr:GFP* (Bloomington Drosophila Stock Center; Pfeiffer et al., 2010), *UAS-GCaMP3* (Bloomington Drosophila Stock Center; Tian et al., 2009), and *UAS-arf6:GFP* (this study). *daughterless*-Gal4 or *tubulin*-Gal4 (Bloomington Drosophila Stock Center) were used to drive ubiquitous expression of all UAS transgenes. *tubulin*-Gal4 was used for all overexpression experiments. *yellow white* flies were used for controls.

Generation of ARF6:GFP

For *UAS-arf6:GFP*, the *arf6* gene was PCR amplified from cDNA (Canadian *Drosophila* Microarray Centre), using 5′-AGATATGTCGACGCATTTTTTAGCG-3′ (forward) and 5′-AGTGTTCTCGAGAGCTTATGGTTCGACG-3′ (reverse) primers. The PCR product was cloned into the Gateway entry vector (Invitrogen) and recombined into the Gateway destination vector pPWG (Invitrogen), containing a C-terminal EGFP tag and an upstream UASp sequence. The destination vector was inserted into the genome using P-element transposon technology (Genetic Services Inc.). A recovered homozygous-viable transgenic fly line containing the transgene on the third chromosome was used for this study.

Time-lapse imaging

Stage 14–15 embryos were dechorionated in 50% bleach for 2 min, aligned with their ventral-lateral side up on an apple juice agar pad,

and transferred to a coverslip coated with heptane glue. Embryos were covered with 1:1 halocarbon oil 27:700 (Sigma-Aldrich) and imaged at 25°C using a Revolution XD spinning disk confocal microscope (Andor Technology) with an iXon Ultra 897 camera (Andor Technology), a 60× oil-immersion lens (NA 1.35; Olympus), and Metamorph software (Molecular Devices). 16-bit Z-stacks were acquired at 0.3-µm steps every 15–60 s and projected for wound closure analysis (15 slices/stack). Wounds were created using a pulsed Micropoint N_2 laser (Andor Technology) tuned to 365 nm.

Drug injections

Embryos were glued onto a coverslip (see Time-lapse imaging), dehydrated for 10–15 min, and covered with 1:1 halocarbon oil 27:700. Pharmacological inhibitors were injected ventrally into the perivitelline space of stage 14–15 embryos using a Transferman NK2 micromanipulator (Eppendorf) and a microinjector (PV820; World Precision Instruments) coupled to our spinning disk confocal microscope. Drugs were injected immediately before wounding and imaging. Drug solutions are predicted to be diluted 50-fold in the embryo (Foe and Alberts, 1983). Dynasore (Tocris Bioscience) was injected at 50 mM in 50% DMSO, chlorpromazine hydrochloride (Sigma-Aldrich) was injected at 50 mM in water, BAPTA (Life Technologies) was injected at 50 mM in water, thapsigargin (Sigma-Aldrich) was injected at 500 µM in 50% DMSO, and Y-27632 (Tocris Bioscience) was injected at 10 mM in water. 50% DMSO and water were used as controls.

Temperature-shift experiments

shi^{ts1}; sqh-GFP:moesin or *shi^{ts1}; sqh-sqh:GFP* (gifts of T. Blankenship, University of Denver, Denver, CO) embryos were dechorionated and transferred to a coverslip, covered with 1:1 halocarbon oil 27:700, and heated at 35°C for 90 min on a hot plate. Embryos were then wounded and imaged. Control *shi^{ts1}* embryos were not heated. Potential effects of temperature on wound healing were controlled for using *sqh-GFP:moesin* or *sqh-sqh:GFP* embryos (not carrying the *shi^{ts1}* mutation) and heated under the same conditions as mutant embryos.

Quantification of E-cadherin expression levels

Embryos were fixed for 1 h in 3.7% formaldehyde in 0.1 M phosphate buffer/heptane (1:1) and manually devitellinized. Antibodies used were rat anti-DCAD2 (1:20; Developmental Studies Hybridoma Bank), mouse anti-Discs large (Dlg; 1:100; Developmental Studies Hybridoma Bank), goat anti–rat IgG conjugated to Alexa Fluor 488 (1:500; Molecular Probes), goat anti–rat IgG conjugated to Alexa Fluor 647 (1:500; Molecular Probes), and goat anti–mouse IgG conjugated to Alexa Fluor 555 (1:400; Invitrogen). Embryos were mounted in Prolong Gold (Molecular Probes). For quantification of E-cadherin levels in embryos expressing endo–E-cadherin:GFP, ubi–E-cadherin:GFP, and UAS–E-cadherin:GFP driven by *tubulin*-Gal4, as well as in *yellow white* embryos injected with water or *shg* dsRNA, embryos were imaged as indicated in the Time-lapse imaging section at 60–100×. Z stacks were acquired at 0.1-µm steps (20–30 slices/stack) and 1–2 slices were projected for quantitative analysis. Cell boundaries were manually delineated in the E-cadherin and Dlg images, and the mean interface fluorescence for each image was calculated after subtracting the image mean as the background. E-cadherin values were normalized to the Dlg values. For quantification of E-cadherin levels in embryos overexpressing UAS-p120-catenin:GFP, embryos were imaged at 25°C using a spinning-disk confocal microscope (Quorum Technologies) with a 63× oil immersion objective (NA 1.4; Carl Zeiss), a piezo top plate, an electron microscopy charge coupled device camera (C9100-13; Hamamatsu Photonics), and Volocity software (PerkinElmer). 16-bit z stacks were acquired at 0.3-µm steps (10–15 slices/stack) and 1–2 slices were projected for quantitative analysis. Image analysis was performed as indicated for the rest of the E-cadherin quantifications.

E-cadherin dsRNA injections

shi^{ts1}; GFP:moesin embryos were collected for 60–90 min at 18°C, glued onto a coverslip, dehydrated for 4–5 min, and covered in 1:1 halocarbon oil 27:700. Embryos were immediately injected ventrally with dsRNA against *shg* at a concentration of 27.5 ng/µl. Water was injected as a control. Templates to produce dsRNA were generated by PCR from genomic DNA with the following primer pairs containing the T7 promoter sequence (5′-TAATACGACTCACTATAGGGAGACCAC-3′) at the 5′ end: *shotgun* T7 forward, 5′-GGACATTATCCTGCAGCGTACCAG-3′; *shotgun* T7 reverse, 5′-CATCGTCCACGTTGGAGTCTGTGTC-3′.

PCR products were used as templates for the T7 transcription reactions with the 5× MEGAscript T7 kit (Ambion). After injection, embryos were incubated at 18°C in a humidified chamber for 18 h, and then heated at 35°C for 90 min on a hot plate. Stage 14–15 embryos were transferred to a drop of heated halocarbon oil 27:700 on a coverslip, mounted on an oxygen-permeable membrane (YSI), and wounded and imaged as indicated in the Time-lapse imaging section. To quantify the degree of E-cadherin knockdown upon dsRNA treatment, control *yellow white* syncytial embryos were injected with *shg* dsRNA or water and aged at 18°C. Embryos were then washed off the coverslip with heptane and fixed and stained with antibodies against E-cadherin and Dlg (see Quantification of E-cadherin expression levels).

Quantitative image analysis

Image analysis was done in SIESTA (Fernandez-Gonzalez and Zallen, 2011), custom software developed in our laboratory using Matlab (MathWorks) and DIPImage (Delft University of Technology). To delineate the wound margin, we used the semiautomated LiveWire algorithm implemented in SIESTA (Fernandez-Gonzalez and Zallen, 2013), in which the user traces the wound margin with the mouse while the algorithm automatically identifies the brightest pixels that follow the trajectory of the mouse. To calculate rates of wound closure, a line was automatically fit to the wound area curve, starting at the initial time point after closure began. The time at which wound closure began was calculated as the time of maximum wound area. The end of the fast phase of wound closure was determined as the time in which the correlation coefficient between the wound area curve and the fitted line was <0.98 (Fernandez-Gonzalez and Zallen, 2013). For experiments in which wound closure was disrupted and there was no fast phase, the rate of closure was calculated between the mean time points in which the fast phase began and ended for the corresponding controls.

To quantify fluorescence at the wound margin, we measured the mean fluorescence of the pixels under a 3-pixel-wide wound outline. Intensity values were background subtracted using the image mode as the background value and corrected for photobleaching by dividing by the mean image intensity at each time point. Total fluorescence was calculated as the product of mean fluorescence by wound perimeter. Intensities were normalized to the mean pixel value in the four time points (1–2 min) before wounding to quantify relative accumulation at the wound margin. Maximum fold enrichment was calculated by averaging the maximum mean or total fluorescence for each one of the movies considered. We quantified the presence of actin-rich structures in rescue experiments by measuring the 90th percentile of the pixel values at the wound margin, instead of the maximum pixel intensity, which is more sensitive to acquisition noise. Similar results were obtained using 70–99th percentiles. Intensities were normalized to the prewounding values.

Analysis of fluorescence dynamics along individual cell edges was done as previously described (Zulueta-Coarasa et al., 2014). In

brief, individual interfaces between wounded and adjacent cells were delineated using the LiveWire annotations. Each interface was divided into 1,000 evenly spaced points and fluorescence was quantified at each of these points using linear interpolation. To account for variation in edge length, points were averaged according to their relative position along the edge. Interface intensity was calculated as the mean of the central 200 points. All intensities were normalized to the values before wounding. Quantification of protrusive activity was done by measuring the fraction of pixels within a 2.4-µm-wide ring inside the wound whose pixel value was greater than the mean image intensity plus 1 standard deviation (for GFP:moesin) or 2.25 standard deviations (for actin:RFP; Zulueta-Coarasa et al., 2014).

Statistical analysis

We compared sample variances using the F-test. To compare mean sample values, we used Student's *t* test for populations with equal or unequal variances (based on the F-test results), applying Holm's correction when more than two groups were considered (Glantz, 2002). For the rescue experiments, time curves were compared using the area under the curve between 20 and 40 min after wounding as the test statistic. Error bars indicate SEM.

Online supplemental material

Fig. S1 shows membrane and cytoplasmic dynamics during embryonic wound repair. Fig. S2 shows that dynasore treatment does not induce apoptosis. Fig. S3 shows that blocking clathrin-mediated endocytosis reduces wound closure rate and that myosin and actin accumulation at the wound margin are impaired in shi^{ts1} embryos at the restrictive temperature. Fig. S4 shows that calcium and actomyosin contractility are required for clathrin accumulation at the wound margin and that thapsigargin treatment impairs wound closure and E-cadherin removal from the wound edge. Fig. S5 shows that overexpressing p120-catenin increases junctional E-cadherin and impairs wound closure. Videos 1–4 show accumulation of myosin (Video 1), clathrin (Video 2), dynamin (Video 3), and ARF6 (Video 4) at the wound margin. Video 5 shows that dynasore treatment prevents rapid wound closure. Video 6 shows that wound closure is impaired in shi^{ts1} embryos at the restrictive temperature. Video 7 shows that BAPTA treatment prevents release of calcium in the epidermis upon wounding. Video 8 shows that calcium signaling is required for the localization of dynamin to the wound margin. Video 9 shows that calcium signaling is required for E-cadherin removal from the wound edge. Online supplemental material is available at http://www.jcb.org/cgi/content/full/jcb.201501076/DC1.

Acknowledgments

We are grateful to Todd Blankenship, Nicole Gorfinkiel, Sérgio Simoes, and Ulli Tepass for reagents and to Teresa Zulueta-Coarasa for help with quantitative analysis. We thank Sean Egan and Dorothea Godt for insightful discussions and Graeme Hunter, Milica Radisic, Sérgio Simoes, Anna Kobb, Jessica Yu, and Teresa Zulueta-Coarasa for comments on the manuscript. Flybase provided important information for this study.

This work was supported by a Connaught Fund New Investigator Award to R. Fernandez-Gonzalez and grants from the University of Toronto Faculty of Medicine Dean's New Staff Fund, the Canada Foundation for Innovation (#30279), and the Natural Sciences and Engineering Research Council of Canada Discovery Grant program (#418438-13) to R. Fernandez-Gonzalez.

The authors declare no competing financial interests.

Submitted: 20 January 2015
Accepted: 14 July 2015

References

Abreu-Blanco, M.T., J.M. Verboon, R. Liu, J.J. Watts, and S.M. Parkhurst. 2012. *Drosophila* embryos close epithelial wounds using a combination of cellular protrusions and an actomyosin purse string. *J. Cell Sci.* 125:5984–5997. http://dx.doi.org/10.1242/jcs.109066

Amano, M., M. Ito, K. Kimura, Y. Fukata, K. Chihara, T. Nakano, Y. Matsuura, and K. Kaibuchi. 1996. Phosphorylation and activation of myosin by Rho-associated kinase (Rho-kinase). *J. Biol. Chem.* 271:20246–20249. http://dx.doi.org/10.1074/jbc.271.34.20246

Antunes, M., T. Pereira, J.V. Cordeiro, L. Almeida, and A. Jacinto. 2013. Coordinated waves of actomyosin flow and apical cell constriction immediately after wounding. *J. Cell Biol.* 202:365–379.

Bardet, P.L., G. Kolahgar, A. Mynett, I. Miguel-Aliaga, J. Briscoe, P. Meier, and J.P. Vincent. 2008. A fluorescent reporter of caspase activity for live imaging. *Proc. Natl. Acad. Sci. USA.* 105:13901–13905. http://dx.doi.org/10.1073/pnas.0806983105

Behrndt, M., G. Salbreux, P. Campinho, R. Hauschild, F. Oswald, J. Roensch, S.W. Grill, and C.P. Heisenberg. 2012. Forces driving epithelial spreading in zebrafish gastrulation. *Science.* 338:257–260. http://dx.doi.org/10.1126/science.1224143

Brand, A.H., and N. Perrimon. 1993. Targeted gene expression as a means of altering cell fates and generating dominant phenotypes. *Development.* 118:401–415.

Brock, J., K. Midwinter, J. Lewis, and P. Martin. 1996. Healing of incisional wounds in the embryonic chick wing bud: characterization of the actin purse-string and demonstration of a requirement for Rho activation. *J. Cell Biol.* 135:1097–1107. http://dx.doi.org/10.1083/jcb.135.4.1097

Campos, I., J.A. Geiger, A.C. Santos, V. Carlos, and A. Jacinto. 2010. Genetic screen in *Drosophila melanogaster* uncovers a novel set of genes required for embryonic epithelial repair. *Genetics.* 184:129–140. http://dx.doi.org/10.1534/genetics.109.110288

Carvalho, L., A. Jacinto, and N. Matova. 2014. The Toll/NF-κB signaling pathway is required for epidermal wound repair in *Drosophila*. *Proc. Natl. Acad. Sci. USA.* 111:E5373–E5382. http://dx.doi.org/10.1073/pnas.1408224111

Caswell, P.T., S. Vadrevu, and J.C. Norman. 2009. Integrins: masters and slaves of endocytic transport. *Nat. Rev. Mol. Cell Biol.* 10:843–853. http://dx.doi.org/10.1038/nrm2799

Chang, H.C., S.L. Newmyer, M.J. Hull, M. Ebersold, S.L. Schmid, and I. Mellman. 2002. Hsc70 is required for endocytosis and clathrin function in *Drosophila*. *J. Cell Biol.* 159:477–487. http://dx.doi.org/10.1083/jcb.200205086

Chen, Q., and T.D. Pollard. 2013. Actin filament severing by cofilin dismantles actin patches and produces mother filaments for new patches. *Curr. Biol.* 23:1154–1162. http://dx.doi.org/10.1016/j.cub.2013.05.005

Chen, M.S., R.A. Obar, C.C. Schroeder, T.W. Austin, C.A. Poodry, S.C. Wadsworth, and R.B. Vallee. 1991. Multiple forms of dynamin are encoded by *shibire*, a *Drosophila* gene involved in endocytosis. *Nature.* 351:583–586. http://dx.doi.org/10.1038/351583a0

Chircop, M., C.S. Malladi, A.T. Lian, S.L. Page, M. Zavortink, C.P. Gordon, A. McCluskey, and P.J. Robinson. 2010. Calcineurin activity is required for the completion of cytokinesis. *Cell. Mol. Life Sci.* 67:3725–3737. http://dx.doi.org/10.1007/s00018-010-0401-z

Chircop, M., B. Sarcevic, M.R. Larsen, C.S. Malladi, N. Chau, M. Zavortink, C.M. Smith, A. Quan, V. Anggono, P.G. Hains, et al. 2011. Phosphorylation of dynamin II at serine-764 is associated with cytokinesis. *Biochim. Biophys. Acta.* 1813:1689–1699. http://dx.doi.org/10.1016/j.bbamcr.2010.12.018

D'Souza-Schorey, C., and P. Chavrier. 2006. ARF proteins: roles in membrane traffic and beyond. *Nat. Rev. Mol. Cell Biol.* 7:347–358. http://dx.doi.org/10.1038/nrm1910

Damke, H., T. Baba, D.E. Warnock, and S.L. Schmid. 1994. Induction of mutant dynamin specifically blocks endocytic coated vesicle formation. *J. Cell Biol.* 127:915–934. http://dx.doi.org/10.1083/jcb.127.4.915

Davidson, L.A., A.M. Ezin, and R. Keller. 2002. Embryonic wound healing by apical contraction and ingression in *Xenopus laevis*. *Cell Motil. Cytoskeleton.* 53:163–176. http://dx.doi.org/10.1002/cm.10070

DiCostanzo, D., P.P. Rosen, I. Gareen, S. Franklin, and M. Lesser. 1990. Prognosis in infiltrating lobular carcinoma. An analysis of "classical" and variant tumors. *Am. J. Surg. Pathol.* 14:12–23. http://dx.doi.org/10.1097/00000478-199001000-00002

Eppinga, R.D., E.W. Krueger, S.G. Weller, L. Zhang, H. Cao, and M.A. McNiven. 2012. Increased expression of the large GTPase dynamin 2 potentiates metastatic migration and invasion of pancreatic ductal carcinoma. *Oncogene.* 31:1228–1241. http://dx.doi.org/10.1038/onc.2011.329

Fernandez-Gonzalez, R., and J.A. Zallen. 2011. Oscillatory behaviors and hierarchical assembly of contractile structures in intercalating cells. *Phys. Biol.* 8:045005. http://dx.doi.org/10.1088/1478-3975/8/4/045005

Fernandez-Gonzalez, R., and J.A. Zallen. 2013. Wounded cells drive rapid epidermal repair in the early *Drosophila* embryo. *Mol. Biol. Cell.* 24:3227–3237. http://dx.doi.org/10.1091/mbc.E13-05-0228

Fernandez-Gonzalez, R., S.M. Simoes, J.C. Röper, S. Eaton, and J.A. Zallen. 2009. Myosin II dynamics are regulated by tension in intercalating cells. *Dev. Cell.* 17:736–743. http://dx.doi.org/10.1016/j.devcel.2009.09.003

Foe, V.E., and B.M. Alberts. 1983. Studies of nuclear and cytoplasmic behaviour during the five mitotic cycles that precede gastrulation in *Drosophila* embryogenesis. *J. Cell Sci.* 61:31–70.

Gaggioli, C., S. Hooper, C. Hidalgo-Carcedo, R. Grosse, J.F. Marshall, K. Harrington, and E. Sahai. 2007. Fibroblast-led collective invasion of carcinoma cells with differing roles for RhoGTPases in leading and following cells. *Nat. Cell Biol.* 9:1392–1400. http://dx.doi.org/10.1038/ncb1658

Glantz, S.A. 2002. Primer of Biostatistics. McGraw-Hill, New York. 489 pp.

Gu, C., S. Yaddanapudi, A. Weins, T. Osborn, J. Reiser, M. Pollak, J. Hartwig, and S. Sever. 2010. Direct dynamin–actin interactions regulate the actin cytoskeleton. *EMBO J.* 29:3593–3606. http://dx.doi.org/10.1038/emboj.2010.249

Harrison, M.R., N.S. Adzick, M.T. Longaker, J.D. Goldberg, M.A. Rosen, R.A. Filly, M.I. Evans, and M.S. Golbus. 1990. Successful repair in utero of a fetal diaphragmatic hernia after removal of herniated viscera from the left thorax. *N. Engl. J. Med.* 322:1582–1584. http://dx.doi.org/10.1056/NEJM199005313222207

Hathaway, D.R., and R.S. Adelstein. 1979. Human platelet myosin light chain kinase requires the calcium-binding protein calmodulin for activity. *Proc. Natl. Acad. Sci. USA.* 76:1653–1657. http://dx.doi.org/10.1073/pnas.76.4.1653

Hidalgo-Carcedo, C., S. Hooper, S.I. Chaudhry, P. Williamson, K. Harrington, B. Leitinger, and E. Sahai. 2011. Collective cell migration requires suppression of actomyosin at cell–cell contacts mediated by DDR1 and the cell polarity regulators Par3 and Par6. *Nat. Cell Biol.* 13:49–58. http://dx.doi.org/10.1038/ncb2133

Homem, C.C., and M. Peifer. 2009. Exploring the roles of diaphanous and enabled activity in shaping the balance between filopodia and lamellipodia. *Mol. Biol. Cell.* 20:5138–5155. http://dx.doi.org/10.1091/mbc.E09-02-0144

Huang, J., W. Zhou, W. Dong, A.M. Watson, and Y. Hong. 2009. Directed, efficient, and versatile modifications of the *Drosophila* genome by genomic engineering. *Proc. Natl. Acad. Sci. USA.* 106:8284–8289. http://dx.doi.org/10.1073/pnas.0900641106

Ishiyama, N., S.H. Lee, S. Liu, G.Y. Li, M.J. Smith, L.F. Reichardt, and M. Ikura. 2010. Dynamic and static interactions between p120 catenin and E-cadherin regulate the stability of cell-cell adhesion. *Cell.* 141:117–128. http://dx.doi.org/10.1016/j.cell.2010.01.017

Keen, J.H., M.C. Willingham, and I.H. Pastan. 1979. Clathrin-coated vesicles: isolation, dissociation and factor-dependent reassociation of clathrin baskets. *Cell.* 16:303–312. http://dx.doi.org/10.1016/0092-8674(79)90007-2

Kiehart, D.P., C.G. Galbraith, K.A. Edwards, W.L. Rickoll, and R.A. Montague. 2000. Multiple forces contribute to cell sheet morphogenesis for dorsal closure in *Drosophila*. *J. Cell Biol.* 149:471–490. http://dx.doi.org/10.1083/jcb.149.2.471

Kimura, K., M. Ito, M. Amano, K. Chihara, Y. Fukata, M. Nakafuku, B. Yamamori, J. Feng, T. Nakano, K. Okawa, et al. 1996. Regulation of myosin phosphatase by Rho and Rho-associated kinase (Rho-kinase). *Science.* 273:245–248. http://dx.doi.org/10.1126/science.273.5272.245

Kon, S., K. Tanabe, T. Watanabe, H. Sabe, and M. Satake. 2008. Clathrin dependent endocytosis of E-cadherin is regulated by the Arf6GAP isoform SMAP1. *Exp. Cell Res.* 314:1415–1428. http://dx.doi.org/10.1016/j.yexcr.2007.11.006

Kumar, A., T. Gupta, S. Berzsenyi, and A. Giangrande. 2015. N-cadherin negatively regulates collective *Drosophila* glial migration through actin cytoskeleton remodeling. *J. Cell Sci.* 128:900–912. http://dx.doi.org/10.1242/jcs.157974

Lee, T., and L. Luo. 1999. Mosaic analysis with a repressible cell marker for studies of gene function in neuronal morphogenesis. *Neuron.* 22:451–461. http://dx.doi.org/10.1016/S0896-6273(00)80701-1

Levayer, R., A. Pelissier-Monier, and T. Lecuit. 2011. Spatial regulation of Dia and Myosin-II by RhoGEF2 controls initiation of E-cadherin endocytosis during epithelial morphogenesis. *Nat. Cell Biol.* 13:529–540. http://dx.doi.org/10.1038/ncb2224

Lombaerts, M., T. van Wezel, K. Philippo, J.W.F. Dierssen, R.M.E. Zimmerman, J. Oosting, R. van Eijk, P.H. Eilers, B. van de Water, C.J. Cornelisse, and A.M. Cleton-Jansen. 2006. E-cadherin transcriptional downregulation by promoter methylation but not mutation is related to epithelial-to-mesenchymal transition in breast cancer cell lines. *Br. J. Cancer.* 94:661–671.

Macia, E., M. Ehrlich, R. Massol, E. Boucrot, C. Brunner, and T. Kirchhausen. 2006. Dynasore, a cell-permeable inhibitor of dynamin. *Dev. Cell.* 10:839–850. http://dx.doi.org/10.1016/j.devcel.2006.04.002

Martin, P., and J. Lewis. 1992. Actin cables and epidermal movement in embryonic wound healing. *Nature.* 360:179–183. http://dx.doi.org/10.1038/360179a0

Martin, A.C., M. Kaschube, and E.F. Wieschaus. 2009. Pulsed contractions of an actin–myosin network drive apical constriction. *Nature.* 457:495–499. http://dx.doi.org/10.1038/nature07522

Mason, F.M., M. Tworoger, and A.C. Martin. 2013. Apical domain polarization localizes actin-myosin activity to drive ratchet-like apical constriction. *Nat. Cell Biol.* 15:926–936. http://dx.doi.org/10.1038/ncb2796

Mateus, A.M., N. Gorfinkiel, S. Schamberg, and A. Martinez Arias. 2011. Endocytic and recycling endosomes modulate cell shape changes and tissue behaviour during morphogenesis in *Drosophila*. *PLoS ONE.* 6:e18729. http://dx.doi.org/10.1371/journal.pone.0018729

McCluskey, J., J. Hopkinson-Woolley, B. Luke, and P. Martin. 1993. A study of wound healing in the E11.5 mouse embryo by light and electron microscopy. *Tissue Cell.* 25:173–181. http://dx.doi.org/10.1016/0040-8166(93)90017-F

Millard, T.H., and P. Martin. 2008. Dynamic analysis of filopodial interactions during the zippering phase of *Drosophila* dorsal closure. *Development.* 135:621–626. http://dx.doi.org/10.1242/dev.014001

Miyashita, Y., and M. Ozawa. 2007. Increased internalization of p120-uncoupled E-cadherin and a requirement for a dileucine motif in the cytoplasmic domain for endocytosis of the protein. *J. Biol. Chem.* 282:11540–11548. http://dx.doi.org/10.1074/jbc.M608351200

Mooibroek, M.J., D.F. Michiel, and J.H. Wang. 1987. Clathrin light chains are calcium-binding proteins. *J. Biol. Chem.* 262:25–28.

Morckel, A.R., H. Lusic, L. Farzana, J.A. Yoder, A. Deiters, and N.M. Nascone-Yoder. 2012. A photoactivatable small-molecule inhibitor for light-controlled spatiotemporal regulation of Rho kinase in live embryos. *Development.* 139:437–442. http://dx.doi.org/10.1242/dev.072165

Myster, S.H., R. Cavallo, C.T. Anderson, D.T. Fox, and M. Peifer. 2003. *Drosophila* p120catenin plays a supporting role in cell adhesion but is not an essential adherens junction component. *J. Cell Biol.* 160:433–449. http://dx.doi.org/10.1083/jcb.200211083

Nakai, J., M. Ohkura, and K. Imoto. 2001. A high signal-to-noise Ca^{2+} probe composed of a single green fluorescent protein. *Nat. Biotechnol.* 19:137–141. http://dx.doi.org/10.1038/84397

Nakayama, Y., J.M. Shivas, D.S. Poole, J.M. Squirrell, J.M. Kulkoski, J.B. Schleede, and A.R. Skop. 2009. Dynamin participates in the maintenance of anterior polarity in the *Caenorhabditis elegans* embryo. *Dev. Cell.* 16:889–900. http://dx.doi.org/10.1016/j.devcel.2009.04.009

Nanes, B.A., C. Chiasson-MacKenzie, A.M. Lowery, N. Ishiyama, V. Faundez, M. Ikura, P.A. Vincent, and A.P. Kowalczyk. 2012. p120-catenin binding masks an endocytic signal conserved in classical cadherins. *J. Cell Biol.* 199:365–380. http://dx.doi.org/10.1083/jcb.201205029

Oda, H., and S. Tsukita. 2001. Real-time imaging of cell-cell adherens junctions reveals that *Drosophila* mesoderm invagination begins with two phases of apical constriction of cells. *J. Cell Sci.* 114:493–501.

Palacios, F., L. Price, J. Schweitzer, J.G. Collard, and C. D'Souza-Schorey. 2001. An essential role for ARF6-regulated membrane traffic in adherens junction turnover and epithelial cell migration. *EMBO J.* 20:4973–4986. http://dx.doi.org/10.1093/emboj/20.17.4973

Palacios, F., J.K. Schweitzer, R.L. Boshans, and C. D'Souza-Schorey. 2002. ARF6-GTP recruits Nm23-H1 to facilitate dynamin-mediated endocytosis during adherens junctions disassembly. *Nat. Cell Biol.* 4:929–936. http://dx.doi.org/10.1038/ncb881

Pearse, B.M. 1975. Coated vesicles from pig brain: purification and biochemical characterization. *J. Mol. Biol.* 97:93–98. http://dx.doi.org/10.1016/S0022-2836(75)80024-6

Pfeiffer, B.D., T.T. Ngo, K.L. Hibbard, C. Murphy, A. Jenett, J.W. Truman, and G.M. Rubin. 2010. Refinement of tools for targeted gene expression in *Drosophila*. *Genetics.* 186:735–755. http://dx.doi.org/10.1534/genetics.110.119917

Pfeiffer, B.D., J.W. Truman, and G.M. Rubin. 2012. Using translational enhancers to increase transgene expression in *Drosophila*. *Proc. Natl. Acad. Sci. USA.* 109:6626–6631. http://dx.doi.org/10.1073/pnas.1204520109

Pickering, K., J. Alves-Silva, D. Goberdhan, and T.H. Millard. 2013. Par3/Bazooka and phosphoinositides regulate actin protrusion formation during *Drosophila* dorsal closure and wound healing. *Development.* 140:800–809. http://dx.doi.org/10.1242/dev.089557

Ratheesh, A., and A.S. Yap. 2012. A bigger picture: classical cadherins and the dynamic actin cytoskeleton. *Nat. Rev. Mol. Cell Biol.* 13:673–679. http://dx.doi.org/10.1038/nrm3431

Razzell, W., I.R. Evans, P. Martin, and W. Wood. 2013. Calcium flashes orchestrate the wound inflammatory response through DUOX activation and hydrogen peroxide release. *Curr. Biol.* 23:424–429. http://dx.doi.org/10.1016/j.cub.2013.01.058

Rowlatt, U. 1979. Intrauterine wound healing in a 20 week human fetus. *Virchows Arch. A Pathol. Anat. Histol.* 381:353–361. http://dx.doi.org/10.1007/BF00432477

Royou, A., C. Field, J.C. Sisson, W. Sullivan, and R. Karess. 2004. Reassessing the role and dynamics of nonmuscle myosin II during furrow formation in early *Drosophila* embryos. *Mol. Biol. Cell.* 15:838–850. http://dx.doi.org/10.1091/mbc.E03-06-0440

Samaniego, R., L. Sánchez-Martín, A. Estecha, and P. Sánchez-Mateos. 2007. Rho/ROCK and myosin II control the polarized distribution of endocytic clathrin structures at the uropod of moving T lymphocytes. *J. Cell Sci.* 120:3534–3543. http://dx.doi.org/10.1242/jcs.006296

Schafer, D.A., S.A. Weed, D. Binns, A.V. Karginov, J.T. Parsons, and J.A. Cooper. 2002. Dynamin2 and cortactin regulate actin assembly and filament organization. *Curr. Biol.* 12:1852–1857. http://dx.doi.org/10.1016/S0960-9822(02)01228-9

Scholey, J.M., K.A. Taylor, and J. Kendrick-Jones. 1980. Regulation of non-muscle myosin assembly by calmodulin-dependent light chain kinase. *Nature.* 287:233–235. http://dx.doi.org/10.1038/287233a0

Simões, S., B. Denholm, D. Azevedo, S. Sotillos, P. Martin, H. Skaer, J.C. Hombría, and A. Jacinto. 2006. Compartmentalisation of Rho regulators directs cell invagination during tissue morphogenesis. *Development.* 133:4257–4267. http://dx.doi.org/10.1242/dev.02588

Simões, S.M., J.T. Blankenship, O. Weitz, D.L. Farrell, M. Tamada, R. Fernandez-Gonzalez, and J.A. Zallen. 2010. Rho-kinase directs Bazooka/Par-3 planar polarity during *Drosophila* axis elongation. *Dev. Cell.* 19:377–388. http://dx.doi.org/10.1016/j.devcel.2010.08.011

Song, S., S. Eckerle, D. Onichtchouk, J.A. Marrs, R. Nitschke, and W. Driever. 2013. Pou5f1-dependent EGF expression controls E-cadherin endocytosis, cell adhesion, and zebrafish epiboly movements. *Dev. Cell.* 24:486–501. http://dx.doi.org/10.1016/j.devcel.2013.01.016

Steinhardt, R.A., G. Bi, and J.M. Alderton. 1994. Cell membrane resealing by a vesicular mechanism similar to neurotransmitter release. *Science.* 263:390–393. http://dx.doi.org/10.1126/science.7904084

Suraneni, P., B. Rubinstein, J.R. Unruh, M. Durnin, D. Hanein, and R. Li. 2012. The Arp2/3 complex is required for lamellipodia extension and directional fibroblast cell migration. *J. Cell Biol.* 197:239–251. http://dx.doi.org/10.1083/jcb.201112113

Tian, L., S.A. Hires, T. Mao, D. Huber, M.E. Chiappe, S.H. Chalasani, L. Petreanu, J. Akerboom, S.A. McKinney, E.R. Schreiter, et al. 2009. Imaging neural activity in worms, flies and mice with improved GCaMP calcium indicators. *Nat. Methods.* 6:875–881. http://dx.doi.org/10.1038/nmeth.1398

Troyanovsky, R.B., E.P. Sokolov, and S.M. Troyanovsky. 2006. Endocytosis of cadherin from intracellular junctions is the driving force for cadherin adhesive dimer disassembly. *Mol. Biol. Cell.* 17:3484–3493. http://dx.doi.org/10.1091/mbc.E06-03-0190

Tumusiime, S., M.K. Rana, S.S. Kher, V.B. Kurella, K.A. Williams, J.J. Guidry, D.K. Worthylake, and R.A. Worthylake. 2009. Regulation of ROCKII by localization to membrane compartments and binding to DynaminI. *Biochem. Biophys. Res. Commun.* 381:393–396. http://dx.doi.org/10.1016/j.bbrc.2009.02.056

van der Bliek, A.M., and E.M. Meyerowitz. 1991. Dynamin-like protein encoded by the *Drosophila shibire* gene associated with vesicular traffic. *Nature.* 351:411–414. http://dx.doi.org/10.1038/351411a0

Verboon, J.M., and S.M. Parkhurst. 2015. Rho family GTPase functions in *Drosophila* epithelial wound repair. *Small GTPases.* 6:28–35.

Wang, L.H., K.G. Rothberg, and R.G. Anderson. 1993. Mis-assembly of clathrin lattices on endosomes reveals a regulatory switch for coated pit formation. *J. Cell Biol.* 123:1107–1117. http://dx.doi.org/10.1083/jcb.123.5.1107

Whitby, D.J., and M.W. Ferguson. 1991. The extracellular matrix of lip wounds in fetal, neonatal and adult mice. *Development.* 112:651–668.

Wood, W., A. Jacinto, R. Grose, S. Woolner, J. Gale, C. Wilson, and P. Martin. 2002. Wound healing recapitulates morphogenesis in *Drosophila* embryos. *Nat. Cell Biol.* 4:907–912. http://dx.doi.org/10.1038/ncb875

Wu, X.S., and L.G. Wu. 2014. The yin and yang of calcium effects on synaptic vesicle endocytosis. *J. Neurosci.* 34:2652–2659. http://dx.doi.org/10.1523/JNEUROSCI.3582-13.2014

Xu, S., and A.D. Chisholm. 2011. A Gαq-Ca^{2+} signaling pathway promotes actin-mediated epidermal wound closure in *C. elegans*. *Curr. Biol.* 21:1960–1967. http://dx.doi.org/10.1016/j.cub.2011.10.050

Yamamoto, E., G. Kohama, H. Sunakawa, M. Iwai, and H. Hiratsuka. 1983. Mode of invasion, bleomycin sensitivity, and clinical course in squamous cell carcinoma of the oral cavity. *Cancer.* 51:2175–2180. http://dx.doi.org/10.1002/1097-0142(19830615)51:12<2175::AID-CNCR2820511205>3.0.CO;2-M

Yang, J.Y., C.S. Zong, W. Xia, Y. Wei, M. Ali-Seyed, Z. Li, K. Broglio, D.A. Berry, and M.C. Hung. 2006. MDM2 promotes cell motility and invasiveness by regulating E-cadherin degradation. *Mol. Cell. Biol.* 26:7269–7282. http://dx.doi.org/10.1128/MCB.00172-06

Yoshida, C., and M. Takeichi. 1982. Teratocarcinoma cell adhesion: identification of a cell-surface protein involved in calcium-dependent cell aggregation. *Cell.* 28:217–224. http://dx.doi.org/10.1016/0092-8674(82)90339-7

Zulueta-Coarasa, T., M. Tamada, E.J. Lee, and R. Fernandez-Gonzalez. 2014. Automated multidimensional image analysis reveals a role for Abl in embryonic wound repair. *Development.* 141:2901–2911. http://dx.doi.org/10.1242/dev.106898